Journal of Geophysical Research: Solid Earth

RESEARCH ARTICLE
10.1029/2018JB015468

Key Points:
- Relocated hypocenters are concentrated on several discrete planes and migrate along those planes from deeper to shallower levels
- Earthquakes occur randomly in the initial ~50 days but are temporally clustered in later periods
- These observations suggest that the swarm is caused by the increased pore pressure of rising fluids

Supporting Information:
- Supporting Information S1
- Movie S1
- Movie S2
- Movie S3
- Movie S4

Correspondence to:
K. Yoshida,
keisuke.yoshida.d7@tohoku.ac.jp

Citation:
Yoshida, K., & Hasegawa, A. (2018). Hypocenter migration and seismicity pattern change in the Yamagata-Fukushima border, NE Japan, caused by fluid movement and pore pressure variation. *Journal of Geophysical Research: Solid Earth*, *123*, 5000–5017. https://doi.org/10.1029/2018JB015468

Received 11 JAN 2018
Accepted 18 MAY 2018
Accepted article online 24 MAY 2018
Published online 15 JUN 2018

Hypocenter Migration and Seismicity Pattern Change in the Yamagata-Fukushima Border, NE Japan, Caused by Fluid Movement and Pore Pressure Variation

Keisuke Yoshida[1] and **Akira Hasegawa**[1]

[1]Research Center for Prediction of Earthquakes and Volcanic Eruptions, Graduate School of Science, Tohoku University, Sendai, Japan

Abstract The spatiotemporal distributions of hypocenters and temporal change in seismicity patterns were investigated in details for events in the Yamagata-Fukushima border earthquake swarm, which was a remotely triggered earthquake sequence by the 2011 Tohoku-Oki earthquake. We relocated the hypocenters by applying the double-difference location method to differential arrival time data obtained by waveform cross correlations together with the Japan Meteorological Agency catalogue data. The hypocenter distribution obtained clearly shows that the hypocenters are concentrated on several discrete planes and migrate along those planes from deeper to shallower levels instead of diffusing isotropically. Most of the events have nodal planes of focal mechanisms parallel to those discrete planes, suggesting that ruptures of individual events occurred along those macroscopic planes. The timing of earthquake occurrences is almost random during the initial ~50 days, but it gradually becomes temporally clustered in later periods, with the number of events decaying aftershock-like after relatively large events. These observations suggest that the present swarm is caused by a reduction in frictional strength due to the increased pore pressure of fluids rising from greater depths in response to the decrease in arc-normal compressional stress associated with the Tohoku-Oki earthquake. The fluids permeated into several existing planes, reduced frictional strengths, caused the present earthquake swarm, and migrated upward along the planes with the hypocenters. Our previous observations that stress drops are systematically low and b-values are high during the initial ~50 days can be readily explained if the pore pressure is especially high during that period.

1. Introduction

An earthquake occurs when shear stress acting on a plane exceeds the frictional strength of the plane. Based on this definition, we can consider two causes for earthquake occurrences: increases in shear stress and decreases in frictional strength (e.g., Hainzl & Fischer, 2002). Therefore, to understand the earthquake generation mechanism, it is important to grasp not only the evolution of stress but also the behavior of the fluids that affect fault strength. Since an individual earthquake is caused by an increase in stress and/or a reduction in strength, we might expect that the seismicity pattern is also affected by the evolution of stress and pore pressure in the focal area (Hainzl & Ogata, 2005; Llenos et al., 2009; Llenos & Michael, 2013; Roland & McGuire, 2009).

Two typical forms of spatially and temporally clustered seismicity exist: mainshock-aftershock sequences and earthquake swarms. It has been suggested that a reduction in frictional strength due to elevated pore pressure plays an important role in earthquake generation (e.g., Hasegawa, 2017; Hubbert & Rubey, 1959; Miller, 2013; Nur & Booker, 1972; Rice, 1992; Sibson, 1992), both for mainshock-aftershock sequences (e.g., Nur & Booker, 1972) and for earthquake swarms (Nur, 1974; Parotidis et al., 2005; Yamashita, 1999). Mainshock-aftershock sequences are characterized by the decay of seismicity rate in proportion to the reciprocal of time (Omori law), and events are often assumed to be triggered by static stress changes from the mainshock (e.g., King et al., 1994) and other preceding earthquakes (Ogata, 1988). On the other hand, earthquake swarms are often assumed to be caused by aseismic processes, such as aseismic slip (Chen et al., 2012; Roland & McGuire, 2009; Vidale & Shearer, 2006) or fluid migration (e.g., Hainzl & Ogata, 2005). Swarms do not usually exhibit the seismicity rate decay in a manner in line with the Omori law, and no law comparable to the Omori law for mainshock-aftershock sequences is known for swarms.

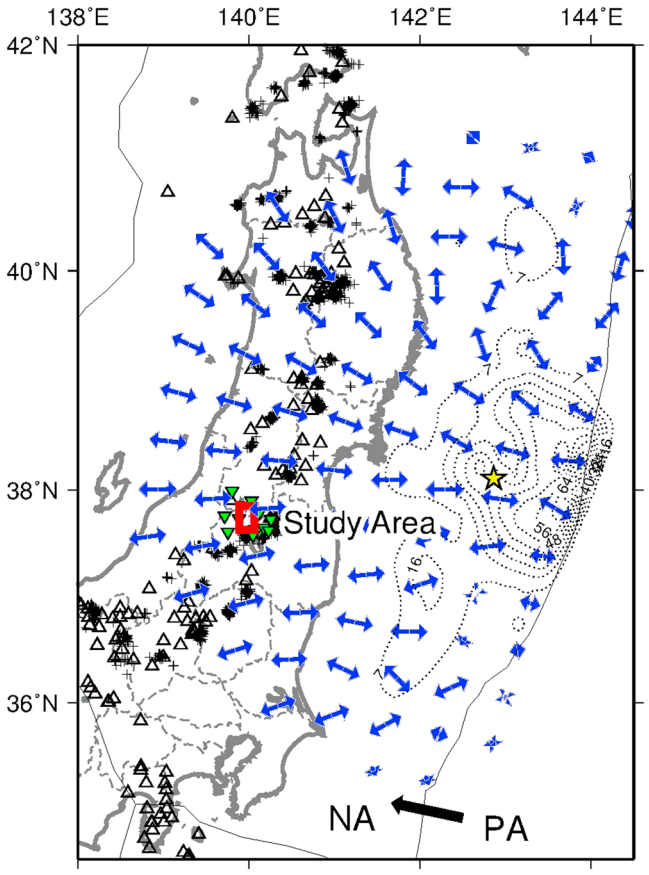

Figure 1. Map showing the location of the study region. The study area is indicated by the red rectangle. The yellow star and dotted contours show the hypocenter and coseismic slip distribution of the 2011 Tohoku-Oki earthquake (Iinuma et al., 2012), respectively. The blue arrows denote the orientations of the σ3 axis of the static stress change caused by the earthquake. Static stress change is estimated at a depth of 10 km. The open triangles indicate quaternary volcanoes.

Fluid-injection-induced-seismicity can be understood to be caused by a reduction in frictional strength due to elevated pore pressure. These events are regarded fundamentally as being no different from natural earthquakes (e.g., Cox, 2016; Hill, 1977; Sibson, 1996). In contrast, the occurrence of at least some earthquake swarms can be explained by a mechanism similar to fluid-injection-induced-seismicity, that is, the reduction in frictional strength due to migrating fluids. The migration behavior of hypocenters, which is frequently seen in earthquake swarms, might provide valuable information on the behavior of fluids within the crust. Since the migration behavior is similar to that observed in fluid-injection-induced-seismicity (e.g., Julian et al., 2010; Parotidis et al., 2005), those earthquake swarms are interpreted as being associated with pore pressure diffusion (e.g., Shapiro et al., 1997). We would expect to obtain some information on fluid behavior and fluid transport properties in the crust by examining the migrating swarms in detail. Aseismic slip is another candidate for the cause of earthquake swarms and hypocenter migration (Ando & Imanishi, 2012; Chen et al., 2012; Kato et al., 2012; Lohman & McGuire, 2007; Nishikawa & Ide, 2017; Segall et al., 2006; Takada & Furuya, 2010; Vidale et al., 2006). Such aseismic slip might contribute to earthquake generation in association with fluids (Hainzl, 2004; Ross et al., 2017; Waite & Smith, 2002).

The 2011 M9 Tohoku-Oki earthquake induced many earthquakes around its source area (Asano et al., 2011; Enescu et al., 2012; Ishibe et al., 2011; Kato et al., 2013; Lengliné et al., 2012; Miyazawa, 2011; Okada et al., 2011; Shimojo et al., 2014; Toda et al., 2011; Yukutake et al., 2011; Yukutake et al., 2013). A great number of aftershocks took place even in inland Japan, which is densely covered by a nationwide seismic network with short-period and broadband seismographs, called the Kiban Network. This provides a unique opportunity to study the mechanism of remote aftershock triggering. Previous studies revealed that migrating earthquake swarms are included in those aftershocks (Kosuga, 2014; Okada et al., 2015; Yoshida, Hasegawa, & Yoshida, 2016; Yoshida et al., 2017; Yoshida & Hasegawa, 2018). The Yamagata-Fukushima border earthquake swarm in the inland area of NE Japan, which was triggered seven days after the Tohoku-Oki earthquake, is the most remarkable example. A total of 28,214 earthquakes were detected by the Japan Meteorological Agency (JMA) during an 800-day period following the Tohoku-Oki earthquake (Figures 1, 2, and S1). The source area of this swarm is located just beneath a caldera structure, where it is believed that shallow igneous bodies with hydrothermal fluids exist (Yoshida et al., 2005). This swarm activity is characterized by reverse-fault focal mechanisms with the *P* axis oriented EW or WNW-ESE, despite the reduction in the EW or WNW-ESE compressional stress caused by the earthquake's static stress change (Yoshida et al., 2012), as shown in Figure 1. Previous studies (Okada et al., 2015; Terakawa et al., 2013; Yoshida, Hasegawa, & Yoshida, 2016; Yoshida et al., 2017) suggested that this swarm was generated in response to an increase in pore pressure due to fluids rising from below, which was caused by the decrease in the EW compressional stress associated with the Tohoku-Oki earthquake.

We expect pore pressure changes during fluid diffusion in this earthquake swarm. In fact, temporal variations in frictional strengths, stress drops, and b-values were reported in the source area of this swarm, which can be explained by the pore pressure change (Yoshida, Hasegawa, & Yoshida, 2016; Yoshida et al., 2017). The hypocenters listed in the JMA unified catalogue (Figures 2a and 3) or even those relocated by Okada et al. (2015) are somewhat scattered and show a cloud-like spatial distribution. Such a spatial distribution suggests that the fluids that triggered the present swarm diffused isotropically in the crust rather than by moving along some macroscopic planar structures, similar to some seismicity caused by fluid-injection-induced seismicity (e.g., Rothert & Shapiro, 2003; Shapiro et al., 2005). However, it is possible that this cloud-like distribution is simply a result of the error in the hypocenter determinations, such as those demonstrated in the focal areas of the 2003 M6.3 Northern Miyagi Prefecture earthquake (Umino et al., 2003; Yoshida, Hasegawa, & Okada,

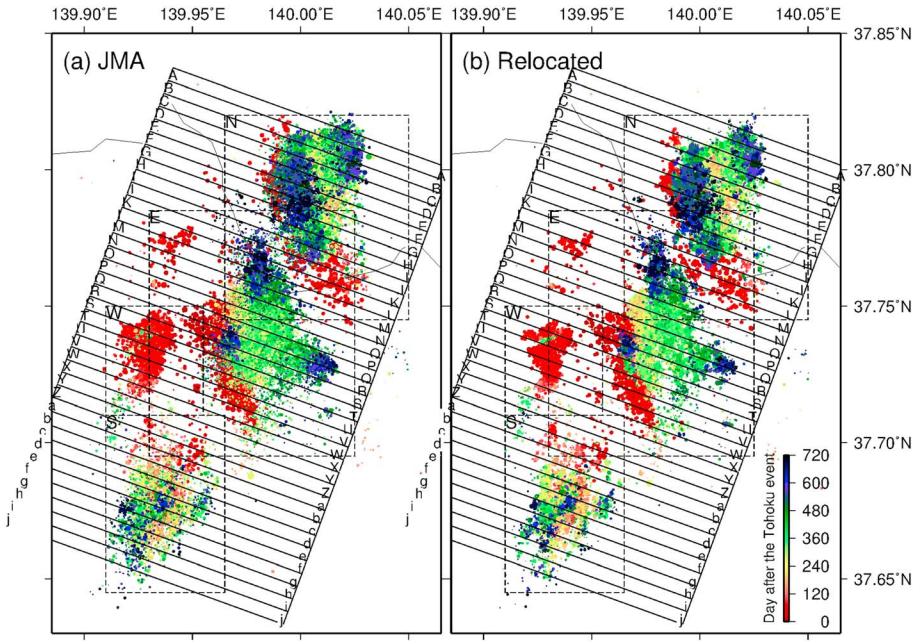

Figure 2. Maps showing the distributions of (a) the original hypocenters listed in the JMA unified catalogue and (b) the relocated hypocenters in this study. The occurrence time of each earthquake is shown by the color scale.

2016), the 2008 M7.2 Iwate-Miyagi Nairiku earthquake (Okada et al., 2012; Yoshida et al., 2014), and the 2011 Sendai-Okura earthquake swarm (Yoshida & Hasegawa, 2018) in central Tohoku.

Thus, the Yamagata-Fukushima border earthquake swarm has several distinct characteristics, which may help deepen our understanding of the generation mechanism of earthquakes and the cause of the diversity in the seismicity patterns. In the present study, we investigate the hypocenter distribution, hypocenter migration, and seismicity pattern change of this swarm in detail. Numerous earthquakes were detected and located by JMA. Focal mechanisms, stress orientations, frictional strengths, stress drops, and b-values have been estimated in details in our previous studies (Yoshida, Hasegawa, & Yoshida, 2016; Yoshida et al., 2017). The focal area is well covered by permanent seismic stations deployed by Tohoku University, JMA, and NIED Hi-net and F-net (Figure 1). By using waveform data obtained by these stations, we were able to precisely relocate the hypocenters of events and investigate hypocenter migrations and seismicity pattern changes.

2. Hypocenter Relocation

We relocated the hypocenters of 28,214 events listed in the JMA catalogue in the focal area of the Yamagata-Fukushima border earthquake swarm. The data period covers 11 March 2011 to 19 May 2013, which are the first 800 days after the 2011 Tohoku-Oki earthquake. The double-difference earthquake relocation method (Waldhauser & Ellsworth, 2000) was applied to arrival time data in the JMA unified catalogue and to differential arrival time data obtained by waveform cross correlations.

The number of differential arrival time data derived from the JMA unified catalogue is 1,174,696 for *P* waves and 1,045,280 for *S* waves. The number of differential arrival time data for *P* and *S* waves derived from waveform cross-correlation delay measurements is 73,669,417 and 42,916,605, respectively. For the waveform correlation measurements, we collected waveform data obtained at nine stations close to the source area (green inverse triangles in Figure 1a), applied a band-pass filter of between 5 and 10 Hz, and computed the cross-correlation function for all the event pairs whose horizontal distances were less than 3.0 km. We adopted the differential arrival times if the cross-correlation coefficient was higher than 0.85. We initially measured the timing of the correlation peak to the nearest sample (0.01 s) and then refined the timing and height of the peak by performing a simple quadratic interpolation as done by Shelly, Hill, et al. (2013). Durations of 2.5 and 4.0 s were adopted for the *P* and *S* wave windows, respectively, starting at 0.3 s before their onsets. The *P* wave window was truncated to avoid overlapping with the *S* wave window when the *S-P* times were

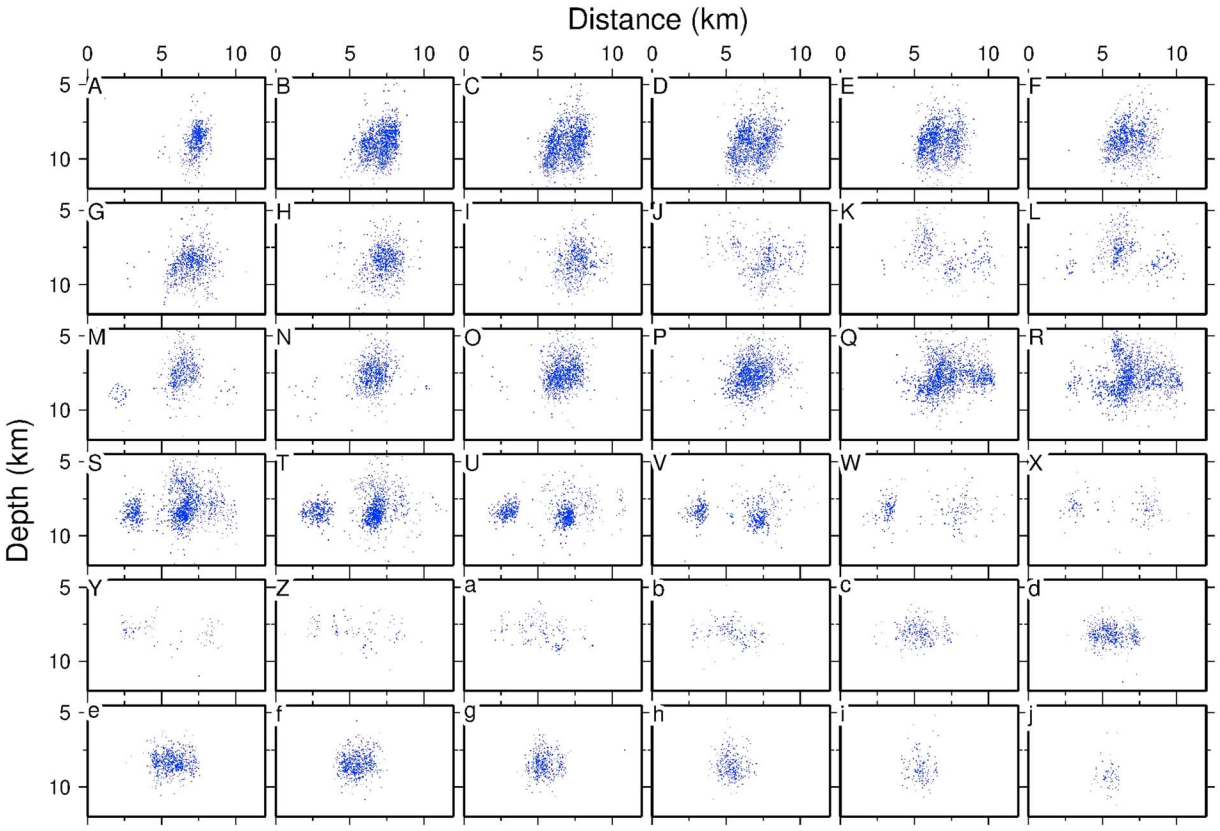

Figure 3. Distribution of the original hypocenters listed in the JMA unified catalogue. Blue dots represent the hypocenters. The 36 figures show across-fault vertical cross-sections along the lines shown in Figure 2.

less than 2.5 s. Manually picked arrival time data listed in the JMA unified catalogue were used if available; otherwise, we used theoretical arrival times computed by assuming the same velocity model as used in the JMA unified catalogue.

For the application of the double-difference location method (Waldhauser & Ellsworth, 2000) to the differential arrival time data obtained above, we used the 1-D velocity model of Hasegawa et al. (1978), which is used routinely at Tohoku University for determining hypocenter locations and focal mechanisms for events in NE Japan. Hypocenters were updated during 50 iterations. In the first half of the iterations, we weighted the catalogue data 10 times stronger than the cross-correlation-derived data to constrain the relative locations at a larger scale ($>$1 km). In the latter half of the iterations, we weighted the cross-correlation-derived data 50 times stronger than the catalogue data to delineate shorter-scale ($<$1 km) structures. The residual of the differential arrival times decreased from 101 to 22 ms during the series of iterations.

3. Results

3.1. Hypocenter Distribution, Focal Mechanisms, and Hypocenter Migration

Distributions of the relocated hypocenters are shown in Figure 2b in map view and in Figure 4 in cross-sectional view. Those of the original JMA locations are shown in Figures 2a and 3, respectively. We can see that the relocated hypocenters are distributed on several thin planes (Figure 4), while the original JMA hypocenters are scattered and show a cloud-like distribution (Figure 3). Such a remarkable change in the hypocenter distribution, from a seismicity cloud to several thin planar structures, is very similar to that observed in the Sendai-Okura earthquake swarm in the central part of NE Japan, which was also triggered by the 2011 Tohoku-Oki earthquake (Yoshida & Hasegawa, 2018). We can attribute the large difference in the spatial distribution between the initial JMA hypocenters and the relocated hypocenters to the difference in the time resolution of arrival time picking.

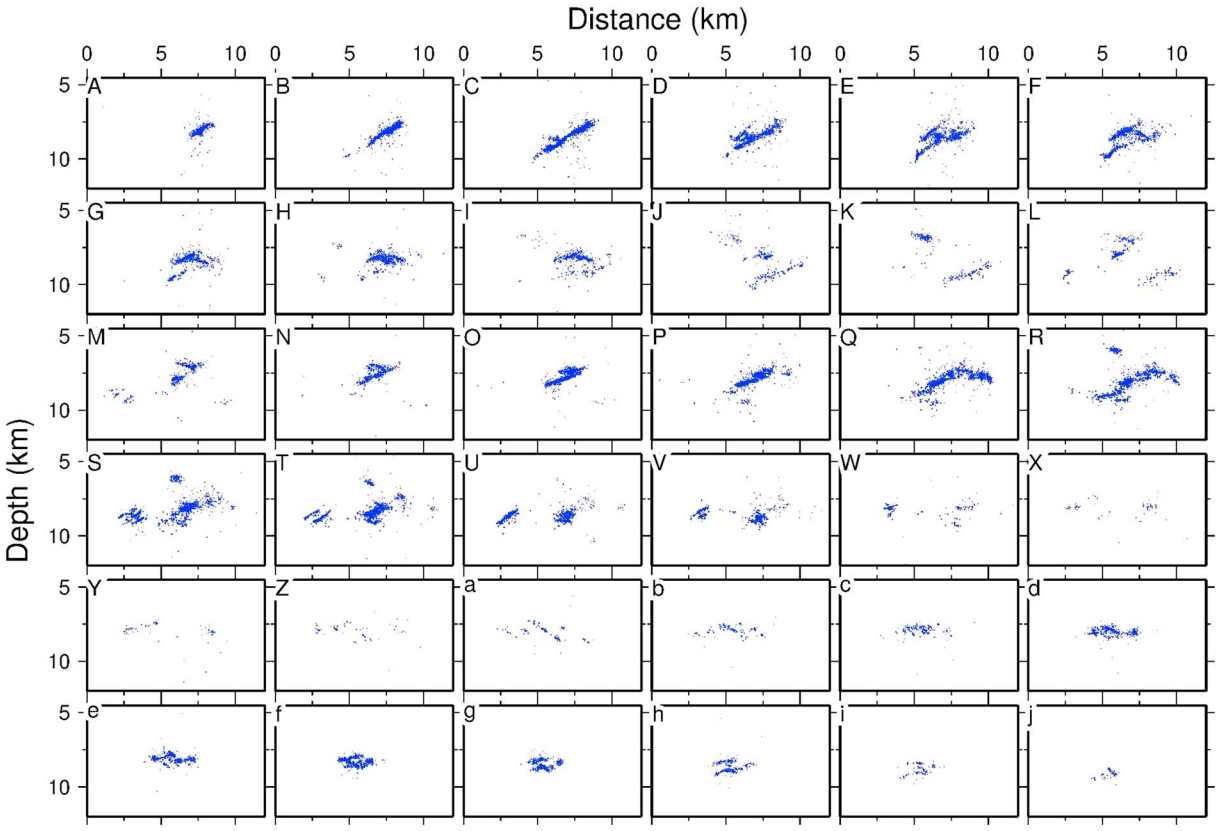

Figure 4. Distribution of the hypocenters relocated in this study. Others are the same as in Figure 3.

Events in the swarm can be divided into four groups from the location of the hypocenters: northern, central, western, and southern clusters. Several macroscopic west dipping alignments of hypocenters (A–G in Figure 4) are evident in the northern cluster. Fault structures seem to become smaller scale and more complicated in the south (H–j) than in the north (A–G). A magnified view of the western cluster is shown in Figure 5. We can see that even this smallest cluster consists of several sharp alignments of hypocenters (Figure 5b). Focal mechanisms determined by Yoshida, Hasegawa, and Yoshida, (2016) are shown in Figure 6. Their west dipping nodal planes are parallel to the alignments of the hypocenters (Figure 6a), which suggests that the ruptures of these individual earthquakes occurred along those macroscopic planes. This observation is similar to that observed in the Sendai-Okura earthquake swarm (Yoshida & Hasegawa, 2018) but is more evident in the present swarm. Magnified views of the other three clusters are shown in Figures 7–9. Videos S1–S4 show animations of the spatial progression of the swarm in the four clusters. Distributions of their focal mechanisms are shown in Figures S2–S4. In these clusters, the hypocenter distributions exhibit slightly more complicated structures but still show similar tendencies to the western cluster. Namely, they tend to occur along the macroscopic planes, and most of events have nodal planes of focal mechanisms parallel to those macroscopic planes.

Hypocenters moved along the planes that were delineated by the precise hypocenter relocations. They moved from deeper to shallower levels, as evident in Figure 10, which shows focal depths plotted against the occurrence time of earthquakes. This hypocenter migration from deeper to shallower levels probably reflects the rise of fluids, suggesting that the present earthquake swarm was caused by a reduction in frictional strength due to fluids rising from the deep crust in response to the decrease of the WNW-ESE compressional stress generated by the 2011 Tohoku-Oki earthquake (Yoshida, Hasegawa, & Yoshida, 2016). In the southern cluster, hypocenters migrated not only to shallower levels but also to deeper levels. Such downward hypocenter migrations have previously been reported by other studies on swarm earthquake activity due to fluid movement (Shelly, Hill, et al., 2013) and controlled induced seismicity (Ake et al., 2005). The groundwater flows in response to pressure differences (e.g., Jaeger et al., 2007). Such downward

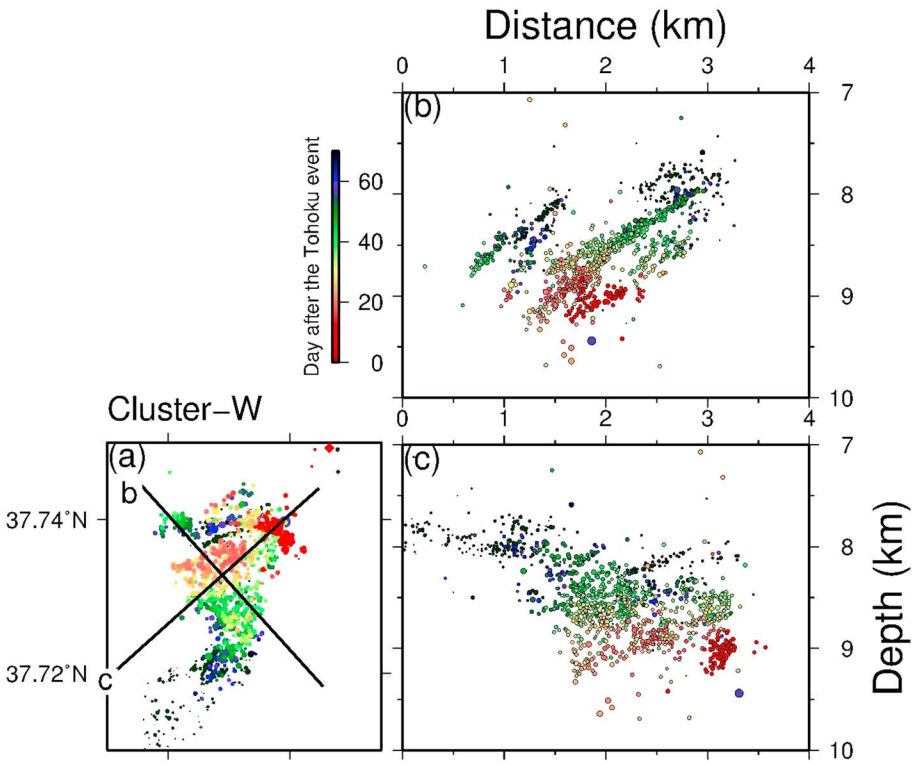

Figure 5. Spatiotemporal evolution of the hypocenters in the western cluster. (a) Map view. (b and c) Cross-sectional views along lines b and c in Figure 5a, respectively. The occurrence time of each earthquake is shown by the color scale.

hypocenter migrations suggest that pore pressure and permeability are strongly heterogeneous in the source region of swarm activity, as suggested by Sibson (1996).

The spatiotemporal evolutions of the hypocenters along five discernible fault planes in the western cluster are shown in Figure 11. The figure clearly shows that the hypocenters migrate from deeper to shallower levels along each plane. The present observation that the hypocenters moved along the individual planes suggests that fluids tend to migrate along planes rather than diffuse in three-dimensional space; this is likely because the permeability is much higher along those preexisting planar structures. We suggest that fluids rising from below following the 2011 Tohoku-Oki earthquake permeated into several thin, preexisting planes, reduced their frictional strengths, activated the earthquake swarm, and caused the migration behavior of hypocenters along the planes accompanied by pore pressure diffusion.

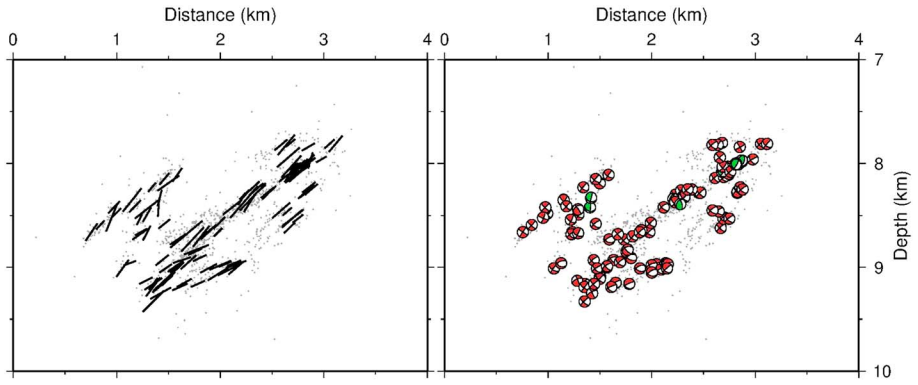

Figure 6. Comparison between the relocated hypocenters and focal mechanisms. Focal mechanisms are shown by "beach balls" in the right figure, and, in the left figure, west dipping nodal planes of focal mechanisms are shown by bars on a vertical cross section along Figure 5's line b. The red, green, and blue beach balls denote thrust, strike-slip, and normal fault types of focal mechanisms whose plunges of the T, P, and B axes were greater than 45°, respectively. Focal mechanisms are those determined by Yoshida, Hasegawa, & Yoshida, (2016).

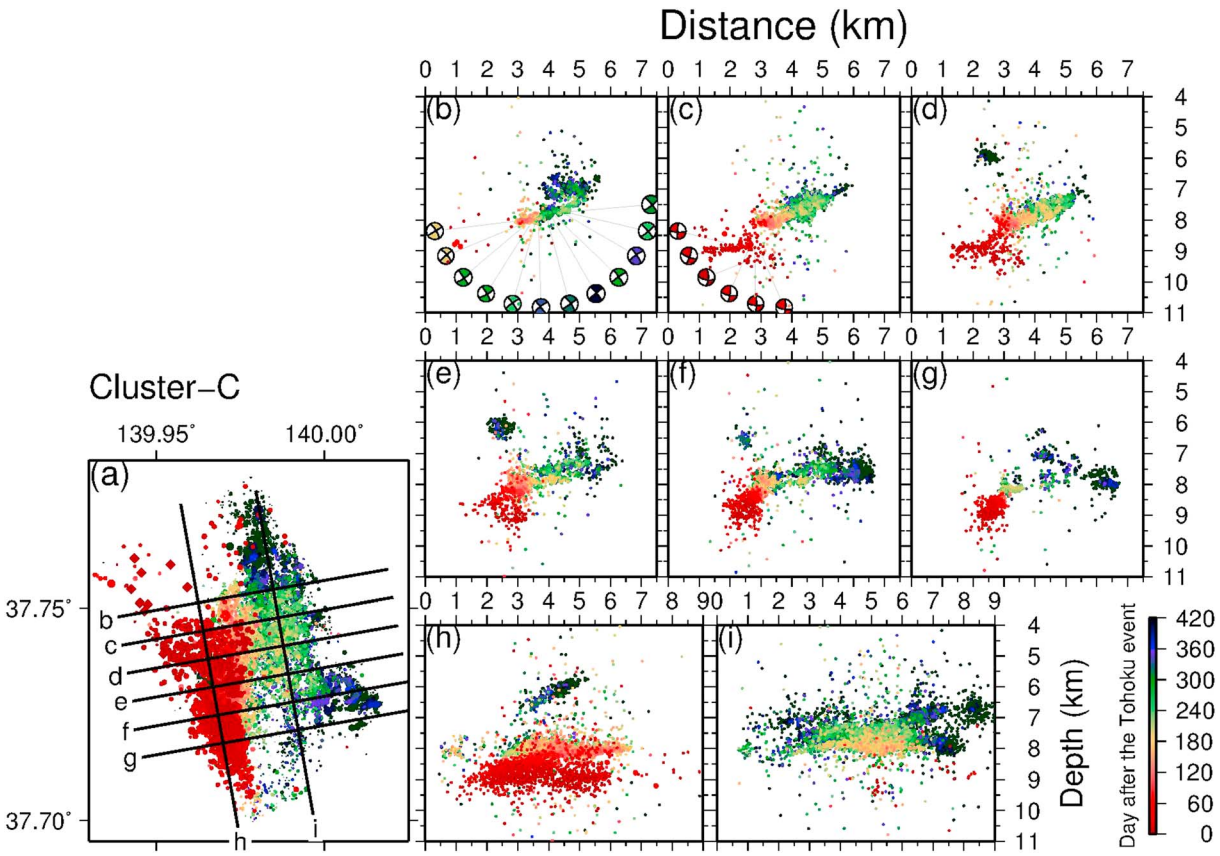

Figure 7. Spatial evolution of hypocenters in the central cluster in (a) map view and (b) to (i) cross-sectional views along lines b to i. The occurrence time of each earthquake is shown by the color scale.

Figure S5 shows the distance of the hypocenter of each earthquake from the mean location of the first five events plotted against time for the four clusters. In the figure, the pore pressure front is also plotted, based on a fluid diffusion model obtained using the following equation (Shapiro et al., 1997):

$$r = \sqrt{4\pi Dt} \tag{1}$$

where r is the distance from the point of pressure source, t is time, and D is hydraulic diffusivity. Envelopes of the hypocenter front of the four clusters can be roughly explained by the fluid diffusion model, with hydraulic diffusivities of 0.2–5.0 m^2/s. This range of hydraulic diffusivity falls within the typical range of 0.1–10 m^2/s (Talwani et al., 2007) obtained by the migration velocities of hypocenters for more than 90 cases of induced seismicity. Hydraulic diffusivities estimated in the source regions of the migrating swarms tend to coincide with this range (Hainzl & Ogata, 2005; Hill & Prejean, 2005; Parotidis et al., 2003, 2005; Shelly, Hill, et al., 2013; Shelly, Moran, et al., 2013; Yukutake et al., 2011), although some do show smaller values ($<$0.1 m^2/s; Chen et al., 2012; Kosuga, 2014; Okada et al., 2015; Yoshida & Hasegawa, 2018).

The observed migration velocity for the present swarm, however, largely varies with time and, hence, with location. The migrating velocity is much higher in the first ~50 days, and a hydraulic diffusivity of $>$1–5 m^2/s is required to explain this velocity. In fact, the synthetic envelope curve is strongly affected by the incident angle of the pore pressure front. Lower values of hydraulic diffusivity can explain the rapid movement of the hypocenters, if we assume that the fluid pressure source is a few kilometers beneath the focal region and the diffusion started a few tens of days before the initiation of the seismicity. However, since this swarm activity started within a week after the 2011 Tohoku-Oki earthquake, a high value of the hydraulic diffusivity ($>$a few m^2/s) is necessary to explain the observed hypocenter migration during this period. This period corresponds to that with very high pore pressure and high seismicity (Yoshida, Hasegawa, & Yoshida, 2016). On the other hand, a hydraulic diffusivity of $<$0.5 m^2/s almost explains the observed migration velocity in the

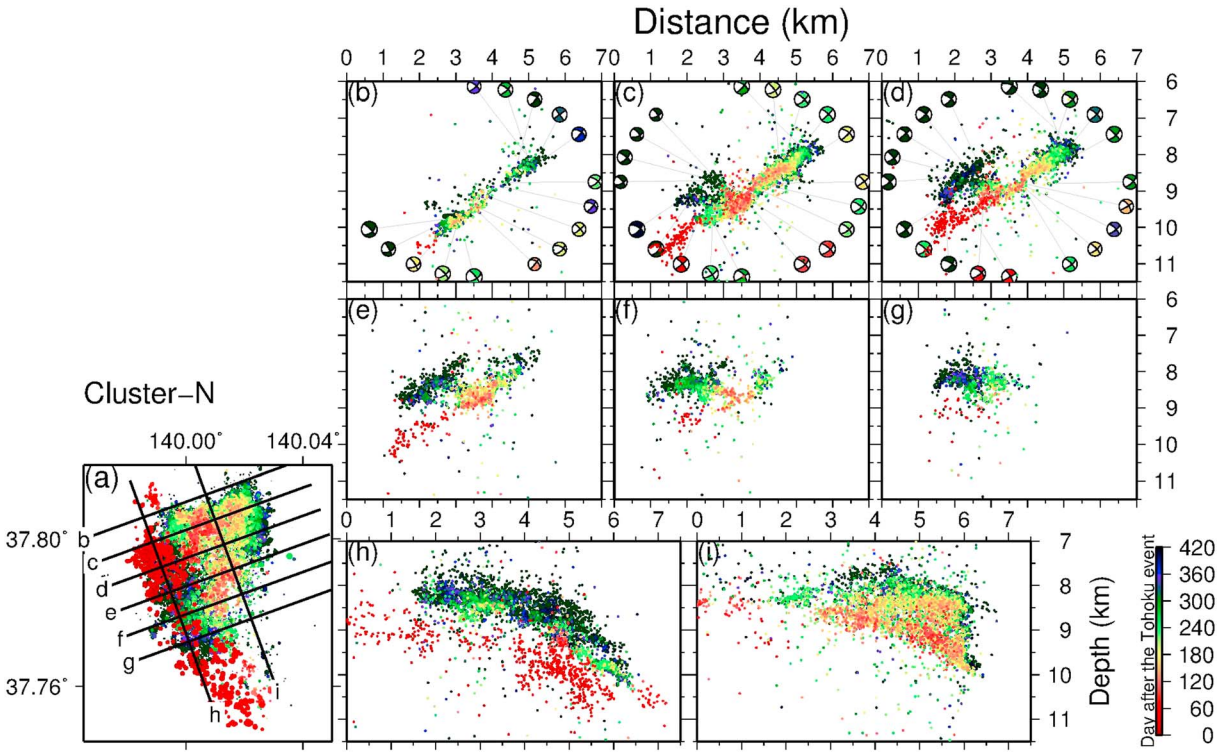

Figure 8. Spatial evolution of the hypocenters in the northern cluster. Others are the same as in Figure 7.

period after ~100 days. The hydraulic diffusivity in this period is relatively small compared to the values identified in previous studies (Shelly, Hill, et al., 2013; Shelly, Moran, et al., 2013; Yukutake et al., 2011), but it is similar to those values observed in the source regions of other migrating swarms triggered after the 2011 Tohoku-Oki earthquake (Kosuga , 2014; Okada et al., 2015; Yoshida & Hasegawa, 2018).

Precise hypocenter determinations in the present study revealed that many earthquakes shared the same fault planes. Yoshida et al. (2017) obtained 1–5 MPa of stress drops for events in this swarm activity, based on the circular crack model proposed by Sato and Hirasawa (1973). In Figure 11, the fault size of each earthquake is represented by the circle diameter, assuming 10 MPa of stress drop. In many cases, faults of individual

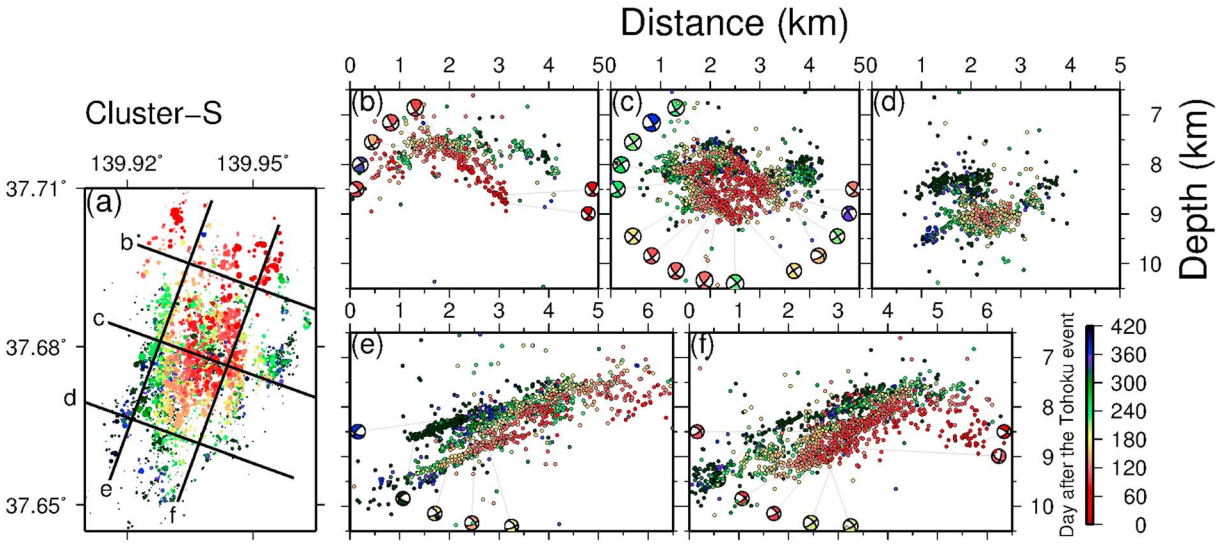

Figure 9. Spatial evolution of the hypocenters in the southern cluster. Others are the same as in Figure 7.

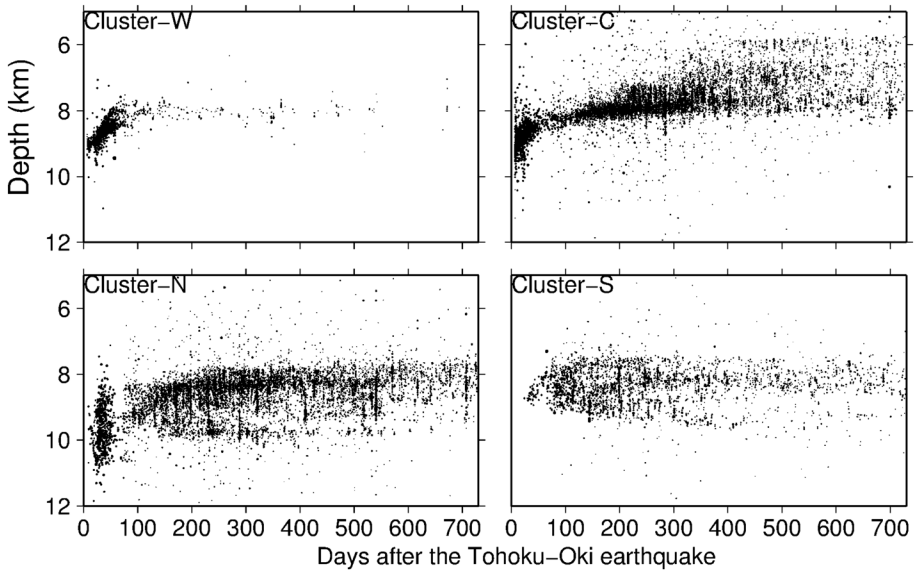

Figure 10. Depth-time plots of the hypocenters of events in the four clusters of the Yamagata-Fukushima border earthquake swarm.

earthquakes overlap each other, even if we assume higher values of stress drop or, more specifically, a shorter fault size length. Some of these earthquakes might have caused repeated slips at the same location on the same fault, which can be explained by repeated increases in pore pressure from rising fluids and/or repeated increases in shear stress by aseismic slip (e.g., Lengliné et al., 2014). The interaction between the earthquakes also

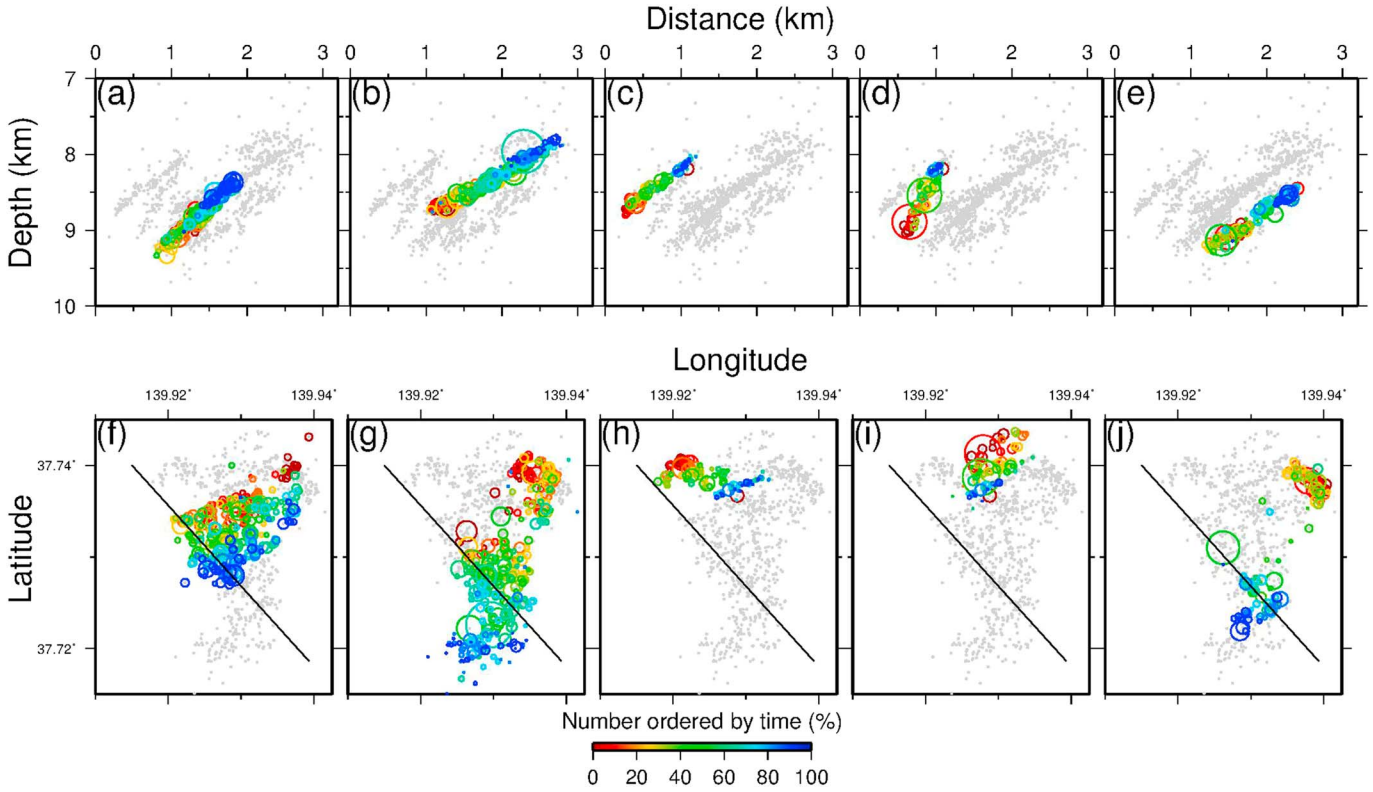

Figure 11. Maps and cross-sectional views showing hypocenter migration along five discrete planes in the western cluster. Hypocenters are shown separately on the five discrete planes from (a), (b), (c), (d), and (e) in map view and on the corresponding planes from (f), (g), (h), (i), and (j) in cross-sectional view along line b in Figure 5a. The color scale shows the sequence of earthquake occurrence ordered by time. The sizes of the circles correspond to the fault diameter, assuming a stress drop of 10 MPa. The gray circles show the hypocenters of other earthquakes.

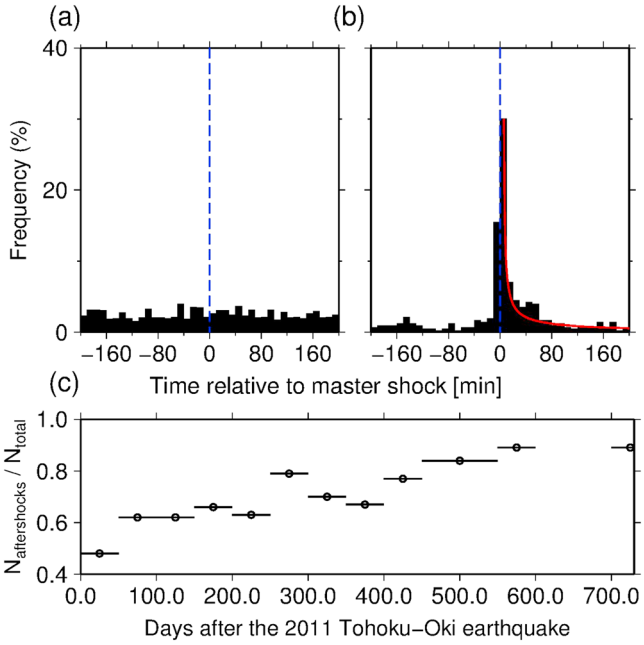

Figure 12. Temporal variations in the seismicity pattern in the source region of the Yamagata-Fukushima border swarm. The stacked timings of aftershocks and foreshocks with magnitudes >2.0 are shown for periods (a) before and (b) after ~50 days from the 2011 Tohoku-Oki earthquake. (c) Temporal variations in the number of aftershocks normalized by that of all the events during that period.

facilitates earthquake occurrence and hypocenter migration. As an example, we show static stress changes caused by the accumulated slips on the five planes in the western cluster in Figure S6. Although earthquakes in the present swarm tend to be small, they increase the shear stress around the area that slipped due to the previous earthquakes, which can trigger nearby aftershocks (e.g., Nandan et al., 2016). The relative importance of the earthquake interactions for the swarm activity increased with time, since pore pressure gradually decreased with time as estimated by Yoshida, Hasegawa, & Yoshida, (2016); this might affect the seismicity pattern, as discussed in the next subsection.

3.2. Seismicity Pattern Change

The earthquake occurrence rate and the spatiotemporal distribution of hypocenters (Figures 10 and S1) suggest that the behavior of the present seismicity seems to differ between two periods: (a) before and (b) after ~50 days from the 2011 Tohoku-Oki earthquake. During period (b), earthquakes tend to occur highly clustered in time, which is visible as many streaks in Figures 10 and S1b that are referred to as bursts. In contrast, during period (a), earthquakes are closely clustered not only in time but also in space, and they do not show streaks. The earthquake occurrence rate is quite high in this period.

To see the differences in the behavior of seismicity from the viewpoint of the classification of the mainshock-aftershock type or swarm earthquake type, we compared time decays of aftershocks between the two periods. Following the method of Hainzl and Fischer (2002), we consider each earthquake to be a "master shock" if it is the largest event in the time interval ($t - T_m$, $t + T_m$). For each master shock, all earthquakes occurring within (t, $t + T_m$) are considered to be aftershocks, whereas events within ($t - T_m$, t) are considered to be foreshocks. The length of the interval is set to $T_m = 200$ (min) for the following calculations. Events with magnitudes >2.5 were adopted as master shocks. Figures 12a and 12b show the stacked timing of aftershock and foreshock occurrences with magnitudes >2.0, which corresponds to the completeness magnitude (Yoshida et al., 2017) during periods (a) and (b), respectively. The results are strikingly different between the two periods. A clear aftershock decay is visible for period (b), and the aftershock number decays following the Omori law (Utsu et al., 1995). In contrast, Omori-like aftershock decay is almost completely obscured in period (a). Bachmann et al. (2011), who analyzed the induced seismicity of the Basel 2006 earthquake sequence, reported that the decay of seismicity can be readily expressed by the Omori law of aftershock decay once the injection stopped. Similarly, our observation might reflect temporal variations in pore pressure.

To observe the temporal change in seismicity patterns, we defined R_{af} as the number of aftershocks normalized by that of all the events during the period. We use R_{af} as an indication of a seismicity pattern; it approaches ~0.5 when the Omori-like decay is completely obscured (swarm-like), whereas it tends to be higher when the Omori-like decay is more evident (aftershock-like). For example, R_{af} is 0.5 for period (a) and 0.8 for period (b). We divided the entire period into 15 time intervals with the same time lengths and plotted them against time in Figure 12c. Calculated R_{af} values are shown in the figure if the number of events is more than 60. The figure clearly shows that R_{af} gradually increases with time from 0.5 to 0.8, which suggests that the swarm-like seismicity pattern gradually changed to the mainshock-aftershock-like seismicity pattern. The change occurred gradually, rather than abruptly, starting from ~50 days after the 2011 Tohoku-Oki earthquake.

If we assume that the Omori-like decay of aftershocks is caused by the effect of stress triggering, seismicity that does not follow the Omori-like decay could be interpreted as caused by external aseismic processes (e.g., Hainzl & Ogata, 2005). Yoshida, Hasegawa, & Yoshida, (2016) estimated from the temporal change in the diversity of earthquake focal mechanisms that pore pressure in the source area increased at first and decreased gradually during the swarm activity due to fluid diffusion. Decreasing pore pressure increases the relative role of stress triggering, which might be responsible for the gradual change in seismicity pattern from the swarm-like to the mainshock-aftershock-like pattern. We suggest that pore pressure changes, which

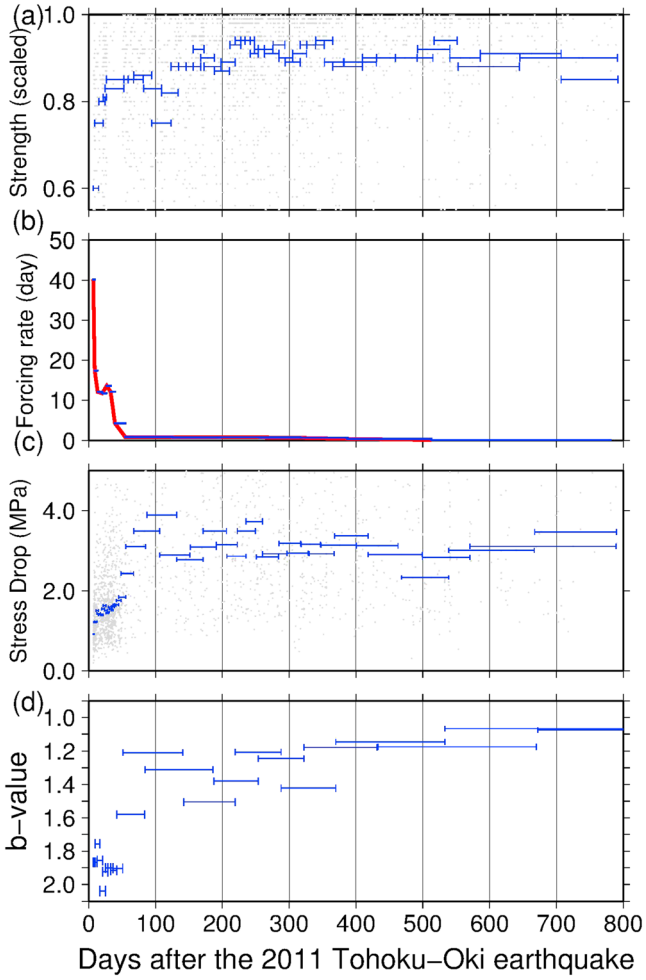

Figure 13. Temporal variations in (a) frictional strength, (b) background seismicity rate, (c) stress drop, and (d) b-value. The horizontal lines show the time periods from which data were taken for computation of the corresponding values. Data for frictional strengths are from Yoshida, Hasegawa, and Yoshida (2016), and those for stress drops and b-values are from Yoshida et al. (2017).

caused this swarm activity, affect not only frictional strengths, stress drops, and b-values, as suggested by Yoshida, Hasegawa, and Yoshida (2016), Yoshida et al. (2017), but also the seismicity pattern itself.

4. Discussion

4.1. Frictional Strength, Stress Drop, and Earthquake Size Distribution

The Yamagata-Fukushima border earthquake swarm is the largest among the migrating earthquake swarms that were triggered in the stress shadow of the 2011 M9 Tohoku-Oki earthquake. This swarm has several distinct characteristics, such as the time delay of the initiation from the Tohoku-Oki earthquake. Detailed investigations of this swarm might provide important insights into the response of seismic behavior under varying pore pressure, that is, frictional strength. Our previous studies found that the diversity of focal mechanisms (Yoshida, Hasegawa, & Yoshida, 2016), stress drops, and b-values (Yoshida et al., 2017) varied with time, probably due to the changes in frictional strengths by the pore pressure variation (Figures 13a, 13c, and 13d). In this study, we further found that (1) hypocenter migration occurs along several planes from deeper to shallower levels and (2) the seismicity pattern changes with time from swarm-like to mainshock-aftershock-like sequences.

The spatial distributions of occurrence times, stress drops, and b-values are shown in Figures 14 and 15, based on the presently relocated hypocenters. The stress drops are those determined by Yoshida et al. (2017). The b-values were obtained at the location of each $M > 2$ event by the maximum likelihood method based on the JMA magnitude, using all the data located within 2 km from the event if there were fewer than 300 events. Otherwise, the 300 events closest to the target event were used. If there were fewer than 100 events, the b-value at that location was not determined. The cutoff magnitude was set at 2.0. We can see a similar pattern of spatial variation among occurrence times, stress drops, and b-values, which reflects the temporal variation in stress drops and b-values (Figures 13c and 13d) due to hypocenter migration.

Yoshida et al. (2017) suggested that the magnitude of the stress drop reflects the frictional strength, on the basis of the observed correlation between the two (Figure 13 in Yoshida et al., 2017). In fact, previous studies reported negative correlations between earthquake stress drops and pore pressure (i.e., positive correlations between stress drops and frictional strengths) based on observations of fluid-injection-induced-seismicity (Goertz-Allmann et al., 2011; Kwiatek et al., 2014; Staszek et al., 2017). Negative correlations between b-values and differential stress were also suggested on the basis of rock experiments and theoretical considerations (Scholz, 1968). Moreover, previous studies found a clear correlation between b-values and pore pressure by investigating fluid-injection-induced-seismicity (Bachmann et al., 2011, 2012; Wyss, 1973). If both the stress drop and b-value reflect the fault strength, then the stress drop and b-value should be related. Thus, we plotted the estimated stress drops against b-values in the Yamagata-Fukushima border earthquake swarm. These are shown by black symbols in Figure 16. As expected, we can recognize a clear negative correlation between the stress drop and b-value (Figure 16).

Such a negative correlation would be obtained if the stress drop is magnitude-dependent, and larger events tend to have higher stress drops than do smaller events (Wyss, 1973). We verified this effect as follows. Estimated stress drops (Yoshida et al., 2017) are plotted against magnitudes (JMA magnitude) and are shown in Figure S7a. The figure shows that stress drops have a notable positive correlation with the JMA magnitude. This correlation perhaps comes mainly from the determination method of the JMA magnitude; it is

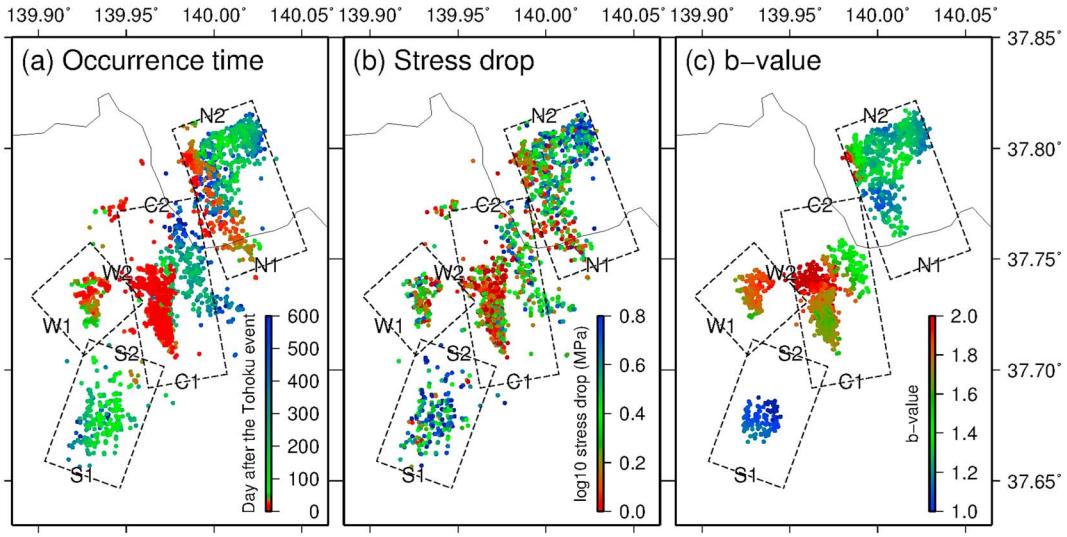

Figure 14. Map views showing (a) occurrence time, (b) stress drops, and (c) b-values. Occurrence time, stress drops, and b-values are shown at the locations of the hypocenters by color scale in each map. The data for the stress drops are from Yoshida et al. (2017).

determined by the seismic moment but is also affected by the predominant frequency. The correlation is largely reduced if we use the moment magnitude determined by the flat level of the displacement source spectra (Figure S7b; Yoshida et al., 2017). The empirical relationship between the stress drop and the JMA magnitude (Figure S7a) is used for removing the effect of the magnitude dependency of stress drops. The correction term for each JMA magnitude is computed as the difference between the mean stress drop at the target magnitude and that of the reference magnitude (M_{JMA} of 2.5 was chosen). Then, the corrected

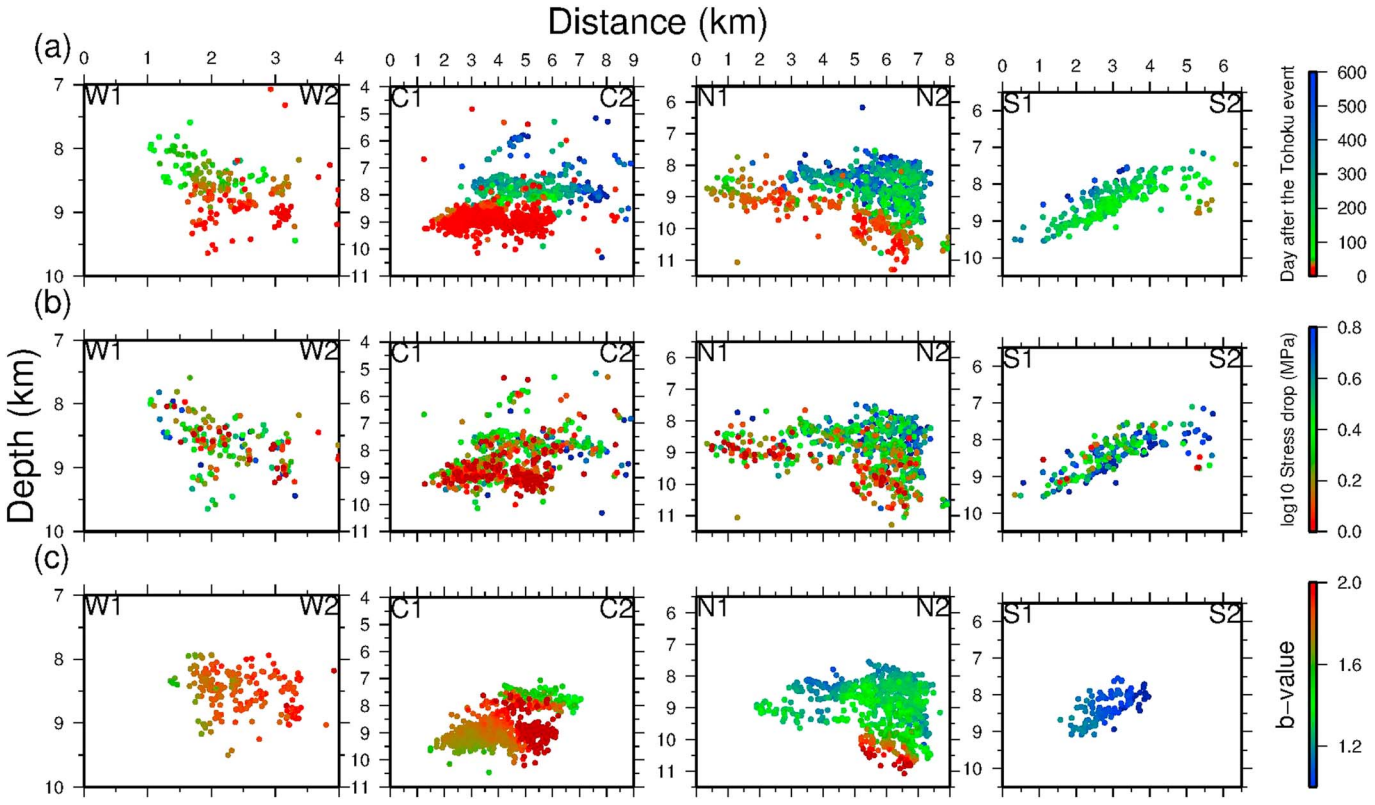

Figure 15. Cross-sectional views showing (a) occurrence time, (b) stress drops, and (c) b-values. Occurrence time, stress drops, and b-values are shown by color scale at the locations of the hypocenters on the vertical cross sections along W1-W2, C1-C2, N1-N2, and S1-S2 in Figure 14. Others are the same as in Figure 14.

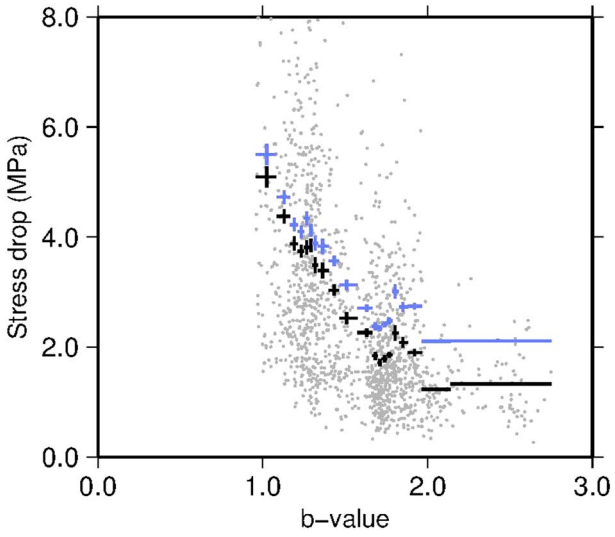

Figure 16. Relationship between stress drops and b-values in the Yamagata-Fukushima border earthquake swarm. The individual values are plotted as gray dots. The median stress drop and b-value are shown by a black plus sign for each bin. The blue plus signs show results for corrected stress drops. The 95% confidence intervals are indicated by vertical bars, and b-values were equally divided into 20 bins according to the stress drop. Each bin has the same number of data points.

value of the stress drop for each earthquake is computed by subtracting the correction term from the observed stress drop. Stress drops thus corrected for the effect of magnitude dependency are plotted against b-values by blue pluses in Figure 16. We can still see a clear negative correlation between the stress drop and b-value. This indicates that the negative correlation between the stress drop and b-value truly exists, regardless of the magnitude dependency of the stress drop. This can also be clearly seen from Figure S8, in which the estimated moment for each event is plotted as a function of corner frequency (Yoshida et al., 2017). We can see that the average value of the stress drops for events for the first 50 days (green symbols) are evidently smaller than those for events after 50 days (black symbols).

4.2. Temporal Variation in the Seismicity Pattern

In section 3.2, we suggested the possibility that the observed temporal change in the seismicity pattern was caused by changes in pore pressure due to fluid diffusion. The temporal change in frictional strength, which has an inverse relationship with pore pressure, was independently estimated based on the diversity of focal mechanisms of the events in this swarm (Yoshida, Hasegawa, & Yoshida, 2016; Figure 13a). The frictional strength was at its lowest in the beginning and gradually increased with time. This temporal pattern can be explained by the very high pore pressure in the beginning and its gradual decrease during the fluid diffusion. In this section, we examine the correlation between the background seismicity rate and independently determined changes in frictional strength. We applied the epidemic-type aftershock sequence (ETAS; Ogata, 1988) to the earthquake catalogue in order to estimate the temporal change in the background seismicity rate by removing the effect of internal stress triggering.

Several researchers have assumed a correlation between seismicity rate and aseismic processes, including the pore pressure change. For example, Nur and Booker (1972) assumed a proportional relationship between seismicity rate and pore pressure change in their discussion of the effect of pore pressure change on aftershock occurrences. In fact, fluid-injection-induced seismicity rate is proportional to the pressure perturbation in fluids filling the pore space in rocks (Shapiro et al., 2005; Shapiro & Dinske, 2009). The ETAS model has been used to extract information on aseismic processes, including the pore pressure change, from seismicity rate (Hainzl & Ogata, 2005; Llenos et al., 2009; Llenos & Michael, 2013; Roland & McGuire, 2009). The ETAS model assumes the seismicity rate to be a summation of the background rate of independent events λ_0 and aftershocks triggered by each event $\lambda_i(t)$:

$$\lambda(t) = \lambda_0 + \sum_{i:t_i<t} \lambda_i(t). \tag{2}$$

Each earthquake can trigger its own aftershock sequence following the modified Omori law (Utsu et al., 1995):

$$\lambda_i(t) = \frac{K_0}{(c + t - t_i)^p} e^{\alpha(M_i - M_{min})}, \tag{3}$$

where t_i is the occurrence time, M_i is the magnitude of each event i that occurred prior to time t, and M_{min} is the magnitude of completeness of the earthquake catalogue; K_0, c, and p are constants, and t is the elapsed time since the main event. The background seismicity rate term λ_0 generally accounts for the effect of tectonic loading but also includes the contribution of external forces, including aseismic processes. Previous studies, which examined the seismicity rate change in response to external forces, focus on the temporal change in the background seismicity rate. Hainzl and Ogata (2005) examined the temporal variation in the background seismicity rate of the 2000 Vogtland/NW Bohemia earthquake swarm by removing the effect of internal stress triggering using the ETAS model. They suggested that the temporal changes in the background seismicity rate thus detected reflected pore pressure changes, based on a physical simulation.

Bachmann et al. (2011) introduced a term proportional to the fluid flow rate in the ETAS model, based on the results of induced seismicity by fluid injection (Shapiro & Dinske, 2009), for the purpose of predicting seismicity rate. Llenos et al. (2009) analyzed seismicity data, which was thought to be affected by aseismic slip, based on the ETAS model. The aseismic slip was independently detected by geodetic observations (Lohman & McGuire, 2007), and Llenos et al. (2009) found that the background seismicity rate changes in response to the stress change were caused by the aseismic slip.

In the present study, we applied the ETAS model by dividing the entire period into several intervals in order to consider the effects of temporal variation in the background seismicity rate. The data set was divided into 14 intervals according to the occurrence times of the earthquakes. Each interval contained the same number (170) of earthquakes. The results suggest that this model almost explains the observed seismicity rate (red curve in Figure S9). Temporal variation in the background seismicity rate is shown by the red curve in Figure 13b. The background seismicity rates showed the highest values in the beginning and gradually decreased with time. This temporal pattern is very consistent with that of frictional strength (Figure 13a), suggesting that seismicity rate and seismicity pattern in the present swarm are affected mainly by changes in pore pressure.

These observations suggest the possibility that information on the evolution of stress and fault strength, which could not be directly estimated from seismological or geodetic data, can be extracted from detailed analyses of seismicity.

4.3. Triggering Mechanism of Migrating Swarms in the Stress Shadow

The Tohoku-Oki earthquake triggered widespread seismicity throughout Japan (e.g., Hirose et al., 2011; Toda et al., 2011). This provides a unique opportunity to study the generation mechanism of aftershocks. The focal mechanisms of most of these events triggered by the Tohoku-Oki earthquake are readily explained by the static stress change caused by the mainshock (e.g., Asano et al., 2011; Chiba et al., 2013; Hasegawa et al., 2011, 2012; Hasegawa & Yoshida, 2015; Nakajima et al., 2013; Yoshida et al., 2012). In contrast, in central Tohoku, NE Japan, the Tohoku-Oki earthquake decreased the EW or ESE-WNW compressional stress, which had prevailed before the Tohoku-Oki earthquake (e.g., Hasegawa et al., 1994; Terakawa & Matsu'ura, 2010; Yoshida et al., 2012, 2015), and the seismicity rate decreased (Suzuki et al., 2014). Nevertheless, the Tohoku-Oki earthquake also triggered some earthquake swarms, such as the Yamagata-Fukushima border swarm, even in central Tohoku (Figure S9), regardless of the reduction in the Coulomb stress (Terakawa et al., 2013; Yoshida et al., 2017, 2012; Yoshida, Hasegawa, & Yoshida, 2016). Those swarms all show a distinct migration behavior of the hypocenters, as summarized by Okada et al. (2015), suggesting the involvement of fluids in the sudden occurrences of seismicity in central Tohoku. The present study revealed that events in the Yamagata-Fukushima border earthquake swarm occurred along several macroscopic planes instead of scattering isotropically, and the hypocenters migrated along those planes from deeper to shallower levels. This observation is very similar to that in the Sendai-Okura earthquake swarm (Yoshida & Hasegawa, 2018), which is another migrating swarm triggered in the stress shadow of the Tohoku-Oki earthquake (Figure S2). Indeed, the Sendai-Okura swarm is considered to be a small version of the Yamagata-Fukushima border swarm. Both the Yamagata-Fukushima border swarm and the Sendai-Okura swarm, which are characterized by reverse-fault focal mechanisms with the P axis oriented EW or WNW-fESE according to the F-fnet moment tensor catalog (Fukuyama et al., 1998; Fukuyama & Dreger, 2003) occurred along geological boundaries (Figure S10), and the caldera structures exist in and around their source regions (Sato et al., 2002; Yoshida, Hasegawa, & Yoshida, 2016). This suggests that the fault-fracture network had been developed by repeated fluid passages under the conditions of structural heterogeneity (Hill, 1977; Sibson, 1996) before the occurrence of the present earthquake swarm.

We suggest that all the swarms in central Tohoku, the stress shadow of the Tohoku-Oki earthquake, were caused by the upward movement of fluids facilitated by the decrease in EW or ESE-WNW compressional stress due to the Tohoku-Oki earthquake. Breaking of low-permeability seals due to the ground shaking might have helped fluid move to the shallower levels. The fluids permeated into several preexisting planes, reduced the frictional strengths, and satisfied the failure criteria, causing the earthquake swarms despite the reduction in the Coulomb stress. The fluids probably further migrated upward along the planes, which manifested as the hypocenters migrating along the planes. Also, interactions between earthquakes and possible slow slips might facilitate earthquake occurrences and hypocenter migrations along preexisting faults.

The temporal evolution of pore pressure due to the migrating fluids not only caused the hypocenter migration but also affected the diversity of the focal mechanisms (Yoshida, Hasegawa, & Yoshida, 2016), the stress drops of individual earthquakes, and the earthquake size distribution (Yoshida et al., 2017), as summarized in Figure 13. These observations are very similar to the temporal changes observed in fluid-injection-experiments (e.g., Bachmann et al., 2011, 2012; Kwiatek et al., 2014; Martínez-Garzón et al., 2014; Staszek et al., 2017), suggesting that the generation mechanism of the Yamagata-Fukushima border swarm is essentially similar to the fluid-injection-induced seismicity. This similarity supports the hypothesis that those swarms that occurred in the stress shadow were triggered by the migration of fluids. We attribute these three independent observations to the upward movement of fluid along preexisting planes due to the decrease in E-W or ESE-WNW compressional stress caused by the Tohoku-Oki earthquake. Since the overpressure fluid source is not infinite, increased pore pressure should gradually decrease as the diffusion proceeds. The present observations (Figure 13) suggest that the pore fluid pressure was high enough to activate less favorably oriented fault planes and cause anomalously large b-values for the initial 50 days. Although not so high compared with the initial 50 days, the seismicity is still high, and the hypocenter migration continues even after 50 days. This is because the fluid movement continued, but the degree of excess pore fluid pressure decreased for the period after 50 days to a level at which only favorably oriented fault planes were activated and b-values were not very large.

In general, pore pressure changes accompanied by the occurrence of a large earthquake combined with permeability anisotropy (e.g., Sibson, 1992) have the potential to trigger an aftershock sequence (Nur & Booker, 1972). Such fluid-triggered aftershocks could also occur when a future megathrust earthquake takes place. Detailed knowledge about the spatiotemporal evolution of pore pressure as well as stress is essential to predict aftershock occurrences.

5. Conclusions

We investigated the spatiotemporal distribution of hypocenters and the temporal changes in seismicity patterns in the source area of the Yamagata-Fukushima border earthquake swarm. We first relocated the hypocenters of 28,214 earthquakes in the swarm using the double-difference hypocenter location technique (Waldhauser & Ellsworth, 2000). Precise differential arrival time data were obtained by waveform cross-correlations. As a result, the accuracy of the hypocenter locations significantly improved. The hypocenters showed a cloud-like distribution before the relocation, whereas they are distributed on several planar structures after the relocation. The hypocenters migrate along these several planes, instead of diffusing isotropically, from deeper to shallower levels. Most of the events have nodal planes of focal mechanisms parallel to these macroscopic alignments of hypocenters, suggesting that slips of individual earthquakes are caused using sections of these macroscopic planes.

The seismicity patterns changed with time during the swarm activity. The timing of the earthquake occurrences was almost random during the initial period, but it gradually exhibited a temporally clustered nature, developing aftershock-like decay of seismicity in the later periods. The background seismicity rate, determined by ETAS fitting, showed the highest values in the initial period and gradually decreased with time. This temporal pattern of the background seismicity rate coincides well with that of frictional strengths previously obtained, suggesting that the seismicity rate and seismicity pattern in the present swarm are affected mainly by variations in pore pressure.

We suggest that the present earthquake swarm was triggered by the decrease in frictional strength caused by fluids rising from deeper levels due to the E-W extension produced by the 2011 Tohoku-Oki earthquake. The fluids permeated into several preexisting planes, reduced their frictional strengths, caused the earthquake swarm, and migrated upward with the hypocenters. During this process, the seismicity, diversity of the focal mechanisms (Yoshida, Hasegawa, & Yoshida, 2016), stress drops, and b-values (Yoshida et al., 2017) were all affected by the evolution of pore pressure due to the migrating fluids. These observations are very similar to those observed in fluid-injection-experiments (e.g., Bachmann et al., 2011, 2012; Kwiatek et al., 2014; Martínez-Garzón et al., 2014; Staszek et al., 2017), suggesting that the generation mechanism of the present earthquake swarm is essentially similar to fluid-injection-induced seismicity. This similarity supports the hypothesis that the present swarm was triggered by the migration of fluids. The present

observations show that information on the evolution of stress and frictional strength can be extracted from detailed analyses of seismicity and source parameters of individual earthquakes.

Acknowledgments
We would like to thank the Editor, Y. Ben-Zion, an Associate Editor, and two anonymous reviewers for their constructive comments, which helped to improve the manuscript. The present study was partly supported by MEXT KAKENHI (26109002). K. Y. thanks T. Yoshida for the discussion about the geological features in Tohoku and T. Taira for the discussion about the analyses of seismicity patterns. The figures in the present paper were created using GMT (Wessel & Smith, 1998). Earthquake data are available via JMA website (http://www.data.jma.go.jp/svd/eqev/data/bulletin/index_e.html). Digital waveform data are available via NIED Hi-net website (http://www.hinet.bosai.go.jp/about_data/?LANG=en).

References

Ake, J., Mahrer, K., O'Connell, D., & Block, L. (2005). Deep-injection and closely monitored induced seismicity at Paradox Valley, Colorado. *Bulletin of the Seismological Society of America*, *95*(2), 664–683. https://doi.org/10.1785/0120040072

Ando, R., & Imanishi, K. (2012). Possibility of M-w 9.0 mainshock triggered by diffusional propagation of after-slip from M-w 7.3 foreshock. *Earth, Planets and Space*, *63*(7), 767–771. https://doi.org/10.5047/eps.2011.05.016

Asano, Y., Saito, T., Ito, Y., Shiomi, K., & Hirose, H. (2011). Spatial distribution and focal mechanisms of aftershocks of the 2011 off the Pacific coast of Tohoku earthquake. *Earth, Planets and Space*, *63*(7), 669–673. https://doi.org/10.5047/eps. 2011.06.016

Bachmann, C. E., Wiemer, S., Goertz-Allmann, B. P., & Woessner, J. (2012). Influence of pore-pressure on the event-size distribution of induced earthquakes. *Geophysical Research Letters*, *39*, L09302. https://doi.org/10.1029/2012GL051480

Bachmann, C. E., Wiemer, S., Woessner, J., & Hainzl, S. (2011). Statistical analysis of the induced Basel 2006 earthquake sequence: Introducing a probability-based monitoring approach for Enhanced Geothermal Systems. *Geophysical Journal International*, *186*(2), 793–807. https://doi.org/10.1111/j.1365-246X.2011.05068.x

Chen, X., Shearer, P. M., & Abercrombie, R. E. (2012). Spatial migration of earthquakes within seismic clusters in Southern California: Evidence for fluid diffusion. *Journal of Geophysical Research*, *117*, B04301. https://doi.org/10.1029/2011JB008973

Chiba, K., Iio, Y., & Fukahata, Y. (2013). Detailed stress fields in the focal region of the 2011 off the Pacific coast of Tohoku earthquake—Implication for the distribution of moment release—. *Earth, Planets and Space*, *64*(12), 1157–1165. https://doi.org/10.5047/eps. 2012.07.008

Cox, S. F. (2016). Injection-driven swarm seismicity and permeability enhancement: Implications for the dynamics of hydrothermal ore systems in high fluid-flux, overpressured faulting regimes—An invited paper. *Economic Geology*, *111*(3), 559–587. https://doi.org/10.2113/econgeo. 111.3.559

Enescu, B., Aoi, S., Toda, S., Suzuki, W., Obara, K., Shiomi, K., & Takeda, T. (2012). Stress perturbations and seismic response associated with the 2011 M9.0 Tohoku-oki earthquake in and around the Tokai seismic gap, central Japan. *Geophysical Research Letters*, *39*, L00G28. https://doi.org/10.1029/2012GL051839

Fukuyama, E., & Dreger, D. (2003). Performance test of an automated moment tensor determination system for the future "Tokai" earthquake. *Earth, Planets and Space*, *52*(6), 383–392. https://doi.org/10.1186/BF03352250

Fukuyama, E., Ishida, M., Dreger, D. S., & Kawai, H. (1998). Automated seismic moment tensor determination by using on-line broadband seismic waveforms. *Zisin*, *51*(1), 149–156. https://doi.org/10.4294/zisin1948.51.1_149

Goertz-Allmann, B. P., Goertz, A., & Wiemer, S. (2011). Stress drop variations of induced earthquakes at the Basel geothermal site. *Geophysical Research Letters*, *38*, L09308. https://doi.org/10.1029/2011GL047498

Hainzl, S. (2004). Seismicity patterns of earthquake swarms due to fluid intrusion and stress triggering. *Geophysical Journal International*, *159*(3), 1090–1096. https://doi.org/10.1111/j.1365-246X.2004.02463.x

Hainzl, S., & Fischer, T. (2002). Indications for a successively triggered rupture growth underlying the 2000 earthquake swarm in Vogtland/NW Bohemia. *Journal of Geophysical Research*, *107*(B12), 2338. https://doi.org/10.1029/2002JB001865

Hainzl, S., & Ogata, Y. (2005). Detecting fluid signals in seismicity data through statistical earthquake modeling. *Journal of Geophysical Research*, *110*, B05S07. https://doi.org/10.1029/2004JB003247

Hasegawa, A. (2017). Role of H2O in generating subduction zone earthquakes. *Monographs on Environment, Earth and Planets*, *5*(1), 1–34. https://doi.org/10.5047/meep. 2017.00501.0001

Hasegawa, A., Horiuchi, S., & Umino, N. (1994). Seismic structure of the northeastern Japan convergent margin: A synthesis. *Journal of Geophysical Research*, *99*, 22,295–22,311. https://doi.org/10.1029/93JB02797

Hasegawa, A., Umino, N., & Takagi, A. (1978). Double-planed structure of the deep seismic zone in the northeastern Japan arc. *Tectonophysics*, *47*(1–2), 43–58. https://doi.org/10.1016/0040-1951 (78)90150-6

Hasegawa, A., & Yoshida, K. (2015). Preceding seismic activity and slow slip events in the source area of the 2011 Mw 9.0 Tohoku-Oki earthquake: A review. *Geoscience Letters*, *2*(1), 6. https://doi.org/10.1186/s40562-015-0025-0

Hasegawa, A., Yoshida, K., Asano, Y., Okada, T., Iinuma, T., & Ito, Y. (2012). Change in stress field after the 2011 great Tohoku-Oki earthquake. *Earth and Planetary Science Letters*, *355–356*, 231–243. https://doi.org/10.1016/j.epsl. 2012.08.042

Hasegawa, A., Yoshida, K., & Okada, T. (2011). Nearly complete stress drop in the 2011 Mw 9.0 off the Pacific coast of Tohoku Earthquake. *Earth, Planets and Space*, *63*(7), 703–707.

Hill, D. P. (1977). A model for earthquake swarms. *Journal of Geophysical Research*, *82*, 1347–1352. https://doi.org/10.1029/JB082i008p01347

Hill, D. P., & Prejean, S. (2005). Magmatic unrest beneath Mammoth Mountain, California. *Journal of Volcanology and Geothermal Research*, *146*(4), 257–283. https://doi.org/10.1016/j.jvolgeores.2005.03.002

Hirose, F., Miyaoka, K., Hayashimoto, N., Yamazaki, T., & Nakamura, M. (2011). Outline of the 2011 off the Pacific coast of Tohoku earthquake (Mw 9.0)—Seismicity: foreshocks, mainshock, aftershocks, and induced activity—. *Earth, Planets and Space*, *63*(7), 513–518. https://doi.org/10.5047/eps.2011.05.019

Hubbert, M., & Rubey, W. (1959). Role of fluid pressure in mechanics of overthrust faulting I. Mechanics of fluid-filled porous solids and its application to overthrust faulting. *Geological Society of America Bulletin*, *70*(2), 115–166.

Iinuma, T., Hino, R., Kido, M., Inazu, D., Osada, Y., Ito, Y., et al. (2012). Coseismic slip distribution of the 2011 off the Pacific Coast of Tohoku Earthquake (M9.0) refined by means of seafloor geodetic data. *Journal of Geophysical Research*, *117*, B07409. https://doi.org/10.1029/2012JB009186

Ishibe, T., Shimazaki, K., Satake, K., & Tsuruoka, H. (2011). Change in seismicity beneath the Tokyo metropolitan area due to the 2011 off the Pacific coast of Tohoku earthquake. *Earth, Planets and Space*, *63*(7), 731–735. https://doi.org/10.5047/eps.2011.06.001, https://doi.org/10.5047/eps.2011.06.001

Jaeger, J., Cook, N. G., & Zimmerman, R. (2007). Fundamentals of rock mechanics, 4th edition. *Journal of Chemical Information and Modeling*, *53*. https://doi.org/10.1017/CBO9781107415324.004

Julian, B. R., Foulger, G. R., Monastero, F. C., & Bjornstad, S. (2010). Imaging hydraulic fractures in a geothermal reservoir. *Geophysical Research Letters*, *37*, L07305. https://doi.org/10.1029/2009GL040933

Kato, A., Fukuda, J., & Obara, K. (2013). Response of seismicity to static and dynamic stress changes induced by the 2011 M 9.0 Tohoku-Oki earthquake. *Geophysical Research Letters*, *40*, 3572–3578. https://doi.org/10.1002/grl.50699

Kato, A., Obara, K., Igarashi, T., Tsuruoka, H., Nakagawa, S., & Hirata, N. (2012). Propagation of slow slip leading up to the 2011 Mw 9.0 Tohoku-Oki earthquake. *Science*, *335*(6069), 705–708. https://doi.org/10.1126/science.1215141

King, G., Stein, R., & Lin, J. (1994). Static stress changes and the triggering of earthquakes. *Bulletin of the Seismological Society of America*, *84*(3), 935–593.

Kosuga, M. (2014). Seismic activity near the Moriyoshi-zan volcano in Akita Prefecture, northeastern Japan: Implications for geofluid migration and a midcrustal geofluid reservoir. *Earth, Planets and Space*, *66*(1), 77. https://doi.org/10.1186/1880-5981-66-77

Kwiatek, G., Bulut, F., Bohnhoff, M., & Dresen, G. (2014). High-resolution analysis of seismicity induced at Berlín geothermal field, El Salvador. *Geothermics*, *52*, 98–111. https://doi.org/10.1016/j.geothermics. 2013.09.008

Lengliné, O., Enescu, B., Peng, Z., & Shiomi, K. (2012). Decay and expansion of the early aftershock activity following the 2011, Mw9.0 Tohoku earthquake. *Geophysical Research Letters*, *39*, L18309. https://doi.org/10.1029/2012GL052797

Lengliné, O., Lamourette, L., Vivin, L., Cuenot, N., & Schmittbuhl, J. (2014). Fluid-induced earthquakes with variable stress drop. *Journal of Geophysical Research: Solid Earth*, *119*, 8900–8913. https://doi.org/10.1002/2014JB011282

Llenos, A. L., McGuire, J. J., & Ogata, Y. (2009). Modeling seismic swarms triggered by aseismic transients. *Earth and Planetary Science Letters*, *281*(1–2), 59–69. https://doi.org/10.1016/j.epsl. 2009.02.011

Llenos, A. L., & Michael, A. J. (2013). Modeling earthquake rate changes in Oklahoma and Arkansas: Possible signatures of induced seismicity. *Bulletin of the Seismological Society of America*, *103*(5), 2850–2861. https://doi.org/10.1785/0120130017

Lohman, R. B., & McGuire, J. J. (2007). Earthquake swarms driven by aseismic creep in the Salton Trough, California. *Journal of Geophysical Research*, *112*, B04405. https://doi.org/10.1029/2006JB004596

Martínez-Garzón, P., Kwiatek, G., Sone, H., Bohnhoff, M., Dresen, G., & Hartline, C. (2014). Spatiotemporal changes, faulting regimes, and source parameters of induced seismicity: A case study from The Geysers geothermal field. *Journal of Geophysical Research: Solid Earth*, *119*, 8378–8396. https://doi.org/10.1002/2014JB011385

Miller, S. A. (2013). The role of fluids in tectonic and earthquake processes. *Advances in Geophysics*, *54*, 1–46. https://doi.org/10.1016/B978-0-12-380940-7.00001-9

Miyazawa, M. (2011). Propagation of an earthquake triggering front from the 2011 Tohoku-Oki earthquake. *Geophysical Research Letters*, *38*, L23307. https://doi.org/10.1029/2011GL049795

Nakajima, J., Yoshida, K., & Hasegawa, A. (2013). An intraslab seismic sequence activated by the 2011 Tohoku-oki earthquake: Evidence for fluid-related embrittlement. *Journal of Geophysical Research: Solid Earth*, *118*, 3492–3505. https://doi.org/10.1002/jgrb. 50246

Nandan, S., Ouillon, G., Woessner, J., Sornette, D., & Wiemer, S. (2016). Systematic assessment of the static stress triggering hypothesis using interearthquake time statistics. *Journal of Geophysical Research: Solid Earth*, *121*, 1890–1909. https://doi.org/10.1002/2015JB012212

Nishikawa, T., & Ide, S. (2017). Detection of earthquake swarms at subduction zones globally: Insights into tectonic controls on swarm activity. *Journal of Geophysical Research: Solid Earth*, *122*, 5325–5343. https://doi.org/10.1002/2017JB014188

Nur, A. (1974). Matsushiro, Japan, earthquake swarm: Confirmation of the dilatancy-fluid diffusion model. *Geology*, *2*(5), 217–221. https://doi.org/10.1130/0091-7613(1974)2<217

Nur, A., & Booker, J. R. (1972). Aftershocks caused by pore fluid flow? *Science*, *175*(4024), 885–887. https://doi.org/10.1126/science. 175.4024.885

Ogata, Y. (1988). Statistical models for earthquake occurrences and residual analysis for point processes. *Journal of the American Statistical Association*, *83*(401), 9–27. https://doi.org/10.1080/01621459.1988.10478560

Okada, T., Matsuzawa, T., Umino, N., Yoshida, K., Hasegawa, A., Takahashi, H., et al. (2015). Hypocenter migration and crustal seismic velocity distribution observed for the inland earthquake swarms induced by the 2011 Tohoku-Oki earthquake in NE Japan: Implications for crustal fluid distribution and crustal permeability. *Geofluids*, *15*(1–2), 293–309. https://doi.org/10.1111/gfl. 12112

Okada, T., Umino, N., & Hasegawa, A. (2012). Hypocenter distribution and heterogeneous seismic velocity structure in and around the focal area of the 2008 Iwate-Miyagi Nairiku earthquake, NE Japan—Possible seismological evidence for a fluid driven compressional inversion earthquake. *Earth, Planets and Space*, *64*(9), 717–728. https://doi.org/10.5047/eps.2012.03.005

Okada, T., Yoshida, K., Ueki, S., Nakajima, J., Uchida, N., Matsuzawa, T., et al. (2011). Shallow inland earthquakes in NE Japan possibly triggered by the 2011 off the Pacific coast of Tohoku earthquake. *Earth, Planets and Space*, *63*(7), 749–754. https://doi.org/10.5047/eps.2011.06.027

Parotidis, M., Rothert, E., & Shapiro, S. A. (2003). Pore-pressure diffusion: A possible triggering mechanism for the earthquake swarms 2000 in Vogtland/NW-Bohemia, central Europe. *Geophysical Research Letters*, *30*(20), 2075. https://doi.org/10.1029/2003GL018110

Parotidis, M., Shapiro, S. A., & Rothert, E. (2005). Evidence for triggering of the Vogtland swarms 2000 by pore pressure diffusion. *Journal of Geophysical Research*, *110*, B05S10. https://doi.org/10.1029/2004JB003267

Rice, J. R. (1992). Fault stress states, pore pressure distributions, and the weakness of the San Andreas Fault. In B. Evans & T. F. Wong (Eds.), *Fault Mechanics and Transport Properties of Rocks* (pp. 475–503). New York: Academic Press.

Roland, E., & McGuire, J. J. (2009). Earthquake swarms on transform faults. *Geophysical Journal International*, *178*(3), 1677–1690. https://doi.org/10.1111/j.1365-246X.2009.04214.x

Ross, Z. E., Rollins, C., Cochran, E. S., Hauksson, E., Avouac, J. P., & Ben-Zion, Y. (2017). Aftershocks driven by afterslip and fluid pressure sweeping through a fault-fracture mesh. *Geophysical Research Letters*, *44*, 8260–8267. https://doi.org/10.1002/2017GL074634

Rothert, E., & Shapiro, S. A. (2003). Microseismic monitoring of borehole fluid injections: Data modeling and inversion for hydraulic properties of rocks. *Geophysics*, *68*(2), 685–689. https://doi.org/10.1190/1.1567239

Sato, H., Imaizumi, T., Yoshida, T., Ito, H., & Hasegawa, A. (2002). Tectonic evolution and deep to shallow geometry of Nagamachi-Rifu Active Fault System, NE Japan. *Earth, Planets and Space*, *54*(11), 1039–1043. https://doi.org/10.1186/BF03353298

Sato, T., & Hirasawa, T. (1973). Body wave spectra from propagating shear cracks. *Journal of Physics of the Earth*, *21*(4), 415–431. https://doi.org/10.4294/jpe1952.21.415

Scholz, C. H. (1968). The frequency-magnitude relation of microfracturing in rock and its relation to earthquakes. *Bulletin of the Seismological Society of America*, *58*(1), 399–415. Retrieved from http://www.bssaonline.org/cgi/content/abstract/58/1/399

Segall, P., Desmarais, E. K., Shelly, D., Miklius, A., & Cervelli, P. (2006). Earthquakes triggered by silent slip events on Kīlauea volcano, Hawaii. *Nature*, *442*(7098), 71–74. https://doi.org/10.1038/nature04938

Shapiro, S. A., & Dinske, C. (2009). Fluid-induced seismicity: Pressure diffusion and hydraulic fracturing. *Geophysical Prospecting*, *57*(2), 301–310. https://doi.org/10.1111/j.1365-2478.2008.00770.x

Shapiro, S. A., Huenges, E., & Borm, G. (1997). Estimating the crust permeability from fluid-injection-induced seismic emission at the KTB site. *Geophysical Journal International*, *131*(2), F15–F18. https://doi.org/10.1111/j.1365-246X.1997.tb01215.x

Shapiro, S. A., Rentsch, S., & Rothert, E. (2005). Characterization of hydraulic properties of rocks using probability of fluid-induced microearthquakes. *Geophysics*, *70*(2), F27–F33. https://doi.org/10.1190/1.1897030

Shelly, D. R., Hill, D. P., Massin, F., Farrell, J., Smith, R. B., & Taira, T. (2013). A fluid-driven earthquake swarm on the margin of the Yellowstone caldera. *Journal of Geophysical Research. Solid Earth*, *118*, 4872–4886. https://doi.org/10.1002/jgrb.50362

Shelly, D. R., Moran, S. C., & Thelen, W. A. (2013). Evidence for fluid-triggered slip in the 2009 Mount Rainier, Washington earthquake swarm. *Geophysical Research Letters*, *40*, 1506–1512. https://doi.org/10.1002/grl.50354

Shimojo, K., Enescu, B., Yagi, Y., & Takeda, T. (2014). Fluid-driven seismicity activation in northern Nagano region after the 2011 M9.0 Tohoku-oki earthquake. *Geophysical Research Letters*, *41*, 7524–7531. https://doi.org/10.1002/2014GL061763

Sibson, R. (1992). Implications of fault-valve behaviour for rupture nucleation and recurrence. *Tectonophysics*, *211*(1–4), 283–293. https://doi.org/10.1016/0040-1951 (92)90065-E

Sibson, R. H. (1996). Structural permeability of fluid-driven fault-fracture meshes. *Journal of Structural Geology*, *18*(8), 1031–1042. https://doi.org/10.1016/0191-8141(96)00032-6

Staszek, M., Orlecka-Sikora, B., Leptokaropoulos, K., Kwiatek, G., & Martínez-Garzón, P. (2017). Temporal static stress drop variations due to injection activity at The Geysers geothermal field, California. *Geophysical Research Letters*, *44*, 7168–7176. https://doi.org/10.1002/2017GL073929

Suzuki, Y., Toda, S., Yoshida, K., & Okada, T. (2014). Local receiver fault dependency of seismicity shut down in the 2011 Tohoku-oki stress shadow, In AGU Fall Meeting, San Francisco, Abstracts (S23A–4473).

Takada, Y., & Furuya, M. (2010). Aseismic slip during the 1996 earthquake swarm in and around the Onikobe geothermal area, NE Japan. *Earth and Planetary Science Letters*, *290*(3–4), 302–310. https://doi.org/10.1016/j.epsl. 2009.12.024

Talwani, P., Chen, L., & Gahalaut, K. (2007). Seismogenic permeability, ks. *Journal of Geophysical Research*, *112*, B07309. https://doi.org/10.1029/2006JB004665

Terakawa, T., Hashimoto, C., & Matsu'ura, M. (2013). Changes in seismic activity following the 2011 Tohoku-oki earthquake: Effects of pore fluid pressure. *Earth and Planetary Science Letters*, *365*, 17–24. https://doi.org/10.1016/j.epsl. 2013.01.017

Terakawa, T., & Matsu'ura, M. (2010). The 3-D tectonic stress fields in and around Japan inverted from centroid moment tensor data of seismic events. *Tectonics*, *29*, TC6008. https://doi.org/10.1029/2009TC002626

Toda, S., Stein, R. S., & Lin, J. (2011). Widespread seismicity excitation throughout central Japan following the 2011 M = 9.0 Tohoku earthquake and its interpretation by Coulomb stress transfer. *Geophysical Research Letters*, *38*, L00G03. https://doi.org/10.1029/2011GL047834

Umino, N., Okada, T., & Nakajima, J. (2003). Hypocenter and focal mechanism distributions of aftershocks of July 26 2003 M6.4 northern Miyagi, NE Japan, earthquake revealed by temporary seismic observation. *Earth, Planets and Space*, *55*(12), 719–730. https://doi.org/10.1186/BF03352481

Utsu, T., Ogata, Y., & Matsu'ura, R. S. (1995). The centenary of the Omori formula for a decay law of aftershock activity. *Journal of Physics of the Earth*, *43*(1), 1–33. https://doi.org/10.4294/jpe1952.43.1

Vidale, J. E., Boyle, K. L., & Shearer, P. M. (2006). Crustal earthquake bursts in California and Japan: Their patterns and relation to volcanoes. *Geophysical Research Letters*, *33*, L20313. https://doi.org/10.1029/2006GL027723

Vidale, J. E., & Shearer, P. M. (2006). A survey of 71 earthquake bursts across southern California: Exploring the role of pore fluid pressure fluctuations and aseismic slip as drivers. *Journal of Geophysical Research*, *111*, B05312. https://doi.org/10.1029/2005JB004034

Waite, G. P., & Smith, R. B. (2002). Seismic evidence for fluid migration accompanying subsidence of the Yellowstone caldera. *Journal of Geophysical Research*, *107*(B9), 2177. https://doi.org/10.1029/2001JB000586

Waldhauser, F., & Ellsworth, W. L. (2000). A double-difference earthquake location algorithm: Method and application to the Northern Hayward Fault, California. *Bulletin of the Seismological Society of America*, *90*(6), 1353–1368. https://doi.org/10.1785/0120000006

Wessel, P., & Smith, W. H. F. (1998). New, improved version of generic mapping tools released. *Eos, Transactions, American Geophysical Union*, *79*, 579. https://doi.org/10.1029/98EO00426

Wyss, M. (1973). Towards a physical understanding of the earthquake frequency distribution. *Geophysical Journal of the Royal Astronomical Society*, *31*(4), 341–359. https://doi.org/10.1111/j.1365-246X.1973.tb06506.x

Yamashita, T. (1999). Pore creation due to fault slip in a fluid-permeated fault zone and its effect on seismicity: Generation mechanism of earthquake swarm. *Pure and Applied Geophysics*, *155*(2–4), 625–647. https://doi.org/10.1007/s000240050280

Yoshida, K., & Hasegawa, A. (2018). Sendai-Okura earthquake swarm induced by the 2011 Tohoku-Oki earthquake in the stress shadow of NE Japan: Detailed fault structure and hypocenter migration. *Tectonophysics*, *733*, 132–147. https://doi.org/10.1016/j.tecto.2017.12.031

Yoshida, K., Hasegawa, A., & Okada, T. (2015). Spatial variation of stress orientations in NE Japan revealed by dense seismic observations. *Tectonophysics*, *647*, 63–72. https://doi.org/10.1016/j.tecto. 2015.02.013

Yoshida, K., Hasegawa, A., & Okada, T. (2016). Heterogeneous stress field in the source area of the 2003 M6.4 Northern Miyagi Prefecture, NE Japan, earthquake. *Geophysical Journal International*, *206*(1), 408–419. https://doi.org/10.1093/gji/ggw160

Yoshida, K., Hasegawa, A., Okada, T., & Iinuma, T. (2014). Changes in the stress field after the 2008 M7.2 Iwate-Miyagi Nairiku earthquake in northeastern Japan. *Journal of Geophysical Research: Solid Earth*, *119*, 9016–9030. https://doi.org/10.1002/2014JB011291

Yoshida, K., Hasegawa, A., Okada, T., Iinuma, T., Ito, Y., & Asano, Y. (2012). Stress before and after the 2011 great Tohoku-oki earthquake and induced earthquakes in inland areas of eastern Japan. *Geophysical Research Letters*, *39*, L03302. https://doi.org/10.1029/2011GL049729

Yoshida, K., Hasegawa, A., & Yoshida, T. (2016). Temporal variation of frictional strength in an earthquake swarm in NE Japan caused by fluid migration. *Journal of Geophysical Research: Solid Earth*, *121*, 5953–5965. https://doi.org/10.1002/2016JB013022

Yoshida, K., Saito, T., Urata, Y., Asano, Y., & Hasegawa, A. (2017). Temporal changes in stress drop, frictional strength, and earthquake size distribution in the 2011 Yamagata-Fukushima, NE Japan, earthquake swarm, caused by fluid migration. *Journal of Geophysical Research: Solid Earth*, *122*, 10,379–10,397. https://doi.org/10.1002/2017JB014334,%20Accepted

Yoshida, T., Nakajima, J., Hasegawa, A., Sato, H., Nagahashi, Y., Kimura, J., et al. (2005). Evolution of late Cenozoic magmatism in the NE Honshu Arc and its relation to the crust-mantle structures (in Japanese with English abstract). *Quaternary Research*, *44*(4), 195–216. https://doi.org/10.4116/jaqua.44.195

Yukutake, Y., Ito, H., Honda, R., Harada, M., Tanada, T., & Yoshida, A. (2011). Fluid-induced swarm earthquake sequence revealed by precisely determined hypocenters and focal mechanisms in the 2009 activity at Hakone volcano, Japan. *Journal of Geophysical Research*, *116*, B04308. https://doi.org/10.1029/2010JB008036

Yukutake, Y., Miyazawa, M., Honda, R., Harada, M., Ito, H., Sakaue, M., et al. (2013). Remotely triggered seismic activity in Hakone volcano during and after the passage of surface waves from the 2011 M9.0 Tohoku-Oki earthquake. *Earth and Planetary Science Letters*, *373*, 205–216. https://doi.org/10.1016/j.epsl.2013.05.004